Article

Control of meiotic crossover interference by a proteolytic chaperone network

Heejin Kim[1,7], Jaeil Kim[1,7], Namil Son[1], Pallas Kuo [2,3], Chris Morgan [4], Aurélie Chambon[5], Dohwan Byun [1], Jihye Park[1], Youngkyung Lee[1], Yeong Mi Park[1], John A. Fozard [4], Julie Guérin[5], Aurélie Hurel[5], Christophe Lambing [2,3], Martin Howard [4], Ildoo Hwang [1], Raphael Mercier [6], Mathilde Grelon [5], Ian R. Henderson [2] & Kyuha Choi [1]✉

Meiosis is a specialized eukaryotic division that produces genetically diverse gametes for sexual reproduction. During meiosis, homologous chromosomes pair and undergo reciprocal exchanges, called crossovers, which recombine genetic variation. Meiotic crossovers are stringently controlled with at least one obligate exchange forming per chromosome pair, while closely spaced crossovers are inhibited by interference. In *Arabidopsis*, crossover positions can be explained by a diffusion-mediated coarsening model, in which large, approximately evenly spaced foci of the pro-crossover E3 ligase HEI10 grow at the expense of smaller, closely spaced clusters. However, the mechanisms that control HEI10 dynamics during meiosis remain unclear. Here, through a forward genetic screen in *Arabidopsis*, we identified *high crossover rate3* (*hcr3*), a dominant-negative mutant that reduces crossover interference and increases crossovers genome-wide. *HCR3* encodes J3, a co-chaperone related to HSP40, which acts to target protein aggregates and biomolecular condensates to the disassembly chaperone HSP70, thereby promoting proteasomal degradation. Consistently, we show that a network of HCR3 and HSP70 chaperones facilitates proteolysis of HEI10, thereby regulating interference and the recombination landscape. These results reveal a new role for the HSP40/J3-HSP70 chaperones in regulating chromosome-wide dynamics of recombination via control of HEI10 proteolysis.

Meiotic recombination is initiated by the formation of programmed DNA double-strand breaks that are repaired using homologous chromosomes as templates to generate crossovers or non-crossovers[1,2]. Despite the formation of excess DNA double-strand breaks, only a subset mature into crossovers via DNA repair, resulting in one obligate crossover per chromosome pair and wide spacing between crossovers in most eukaryotes[3]. Two pathways, class I and class II, mediate crossover formation and positioning[3]. The class I pathway facilitates most crossovers and depends on the conserved pro-crossover ZMM proteins (named after *Saccharomyces cerevisiae* Zip1–4, Mer3 and Msh4–5) and the MutL protein homologue 1 (MLH1)–MLH3 heterodimeric endonuclease (MutLγ)[2,3]. ZMM proteins stabilize recombination intermediates such

[1]Department of Life Sciences, Pohang University of Science and Technology, Pohang, Republic of Korea. [2]Department of Plant Sciences, University of Cambridge, Cambridge, UK. [3]Rothamsted Research, Harpenden, UK. [4]John Innes Centre, Norwich Research Park, Norwich, UK. [5]Institut Jean-Pierre Bourgin (IJPB), Université Paris-Saclay, INRAE, AgroParisTech, Versailles, France. [6]Department of Chromosome Biology, Max Planck Institute for Plant Breeding Research, Cologne, Germany. [7]These authors contributed equally: Heejin Kim, Jaeil Kim. ✉e-mail: kyuha@postech.ac.kr

as displacement loops and double Holliday junctions and recruit MutLγ to resolve crossovers[4]. Class I crossovers are subject to interference that spaces adjacent events wider than expected at random[5]. In contrast, class II crossovers are non-interfering and depend on the endonuclease MUS81 (ref. [6]). Non-interfering crossovers are limited by several anti-recombination factors, including the FANCM and RECQ4A/4B helicases in plants[7,8].

Among ZMMs, the ZIP3/HEI10 (Human Enhancer of Invasion-10) family of meiotic SUMO and/or ubiquitin E3 ligases play a key role in controlling interference-sensitive crossover number and position in a dosage-dependent manner[9–17]. HEI10 is initially loaded on early-leptotene chromosomes and becomes gradually enriched on the synaptonemal complex (SC), a proteinaceous structure that assembles between homologous chromosomes[16,18]. In Arabidopsis (Arabidopsis thaliana), HEI10 E3 ligases are proposed to diffuse along the SC and co-localize with hundreds of recombination intermediates as small foci at synapsed early pachytene[18]. Like biomolecular condensates[19], HEI10 proteins eventually concentrate to late-pachytene designated crossover sites as one or a few large foci, at the expense of smaller foci[16,18]. A diffusion-mediated HEI10 coarsening model has been proposed to explain these dynamics, control of crossover number and interference[18]. In Arabidopsis, genetic disruption of SC transverse filament proteins abolishes interference and increases class I crossovers[20,21]. HORMA domain proteins of SC axis elements are required to promote class I crossovers and mediate interference[22,23]. Interfering crossovers are limited by HCR1 (HIGH CROSSOVER RATE1, also named PROTEIN PHOSPHATASE X 1 (PPX1)) which potentially dephosphorylates HEI10 in Arabidopsis[24]. Consistently, posttranslational modifications of pro-crossover factors, such as phosphorylation, SUMOylation, ubiquitination and proteasomal proteolysis, have been implicated in controlling meiotic recombination in S. cerevisiae, Schizosaccharomyces pombe, Caenorhabditis elegans and mouse[17,23,25–31]. However, the molecular mechanisms that mediate the proteolysis and dynamics of HEI10, the key pro-crossover factor during crossover control in plants, are largely unknown.

Results

Genetic identification of hcr3

To identify new regulators of crossover patterning, we performed a high-throughput forward genetic screen for high crossover rate (hcr) mutants using a fluorescent seed recombination reporter line (420) and ethylmethane sulfonate-mediated mutagenesis in Arabidopsis (Fig. 1a and Supplementary Fig. 1)[24]. The hcr3 and hcr3 heterozygous (hcr3/+) plants showed higher 420 crossover frequency than wild-type Columbia-0 (Col), indicating a dosage effect of hcr3 (all $P < 8.76 \times 10^{-6}$) (Fig. 1b and Supplementary Table 1). Using bulk sequencing of hcr3 BC$_1$F$_2$ segregants, we determined that hcr3 harbours a missense mutation (G-to-A) in J3 (At3g44110) (Fig. 1c and Supplementary Fig. 1d). J3 encodes a class A HSP40 (HEAT SHOCK PROTEIN 40) co-chaperone with an N-terminal J domain (J) followed by a glycine and phenylalanine-rich region (G/F), four copies of a CxxCxGxG zinc finger motif (ZnF) and a C-terminal peptide-binding fragment (C) (Fig. 1c)[32]. The hcr3 mutation caused an amino acid substitution from glycine to arginine (G155R) in the first conserved ZnF (Fig. 1c and Supplementary Figs. 2 and 3). Class A HSP40 proteins form dimers through dimerization domains in their C termini (Fig. 1c and Supplementary Fig. 3)[33]. HSP40 dimers provide substrate specificity for the HSP70 chaperone machinery and cooperate with nucleotide exchange factor, HSP90 or HSP100/ClpB family members, to mediate proteome quality control pathways, including protein disaggregation and degradation[32–35].

hcr3 is a dominant-negative allele of J3

To further investigate the role of J3 in meiotic recombination, we obtained two j3 T-DNA insertion mutants, j3-1 and j3-3, which are loss-of-function alleles with no functional transcripts detected in RNA

sequencing (RNA-seq) and reverse transcription with PCR (RT–PCR) analyses (Fig. 1c and Extended Data Fig. 1a–e). Both mutants were recessive and late flowering, as previously observed[36], and showed increased crossover frequencies in 420 and six more fluorescence-tagged line intervals (FTLs)/Col traffic lines (CTLs), compared to wild type (all $P < 1.88 \times 10^{-3}$) (Fig. 1d, Extended Data Figs. 1i,j and 2a,b and Supplementary Tables 2–5). Complementation using a J3 genomic fragment (J3::Myc-J3) reduced 420 crossover frequency of j3-1 (25 cM) to the wild-type level (20 cM) (all $P > 0.1$) (Fig. 1d and Supplementary Table 2). In addition, we observed that both j3-1 and j3-3 exhibited reduced pollen grains per anther (~63%), reduced number of seeds per silique (~81%) and ~30% chromosomal abnormalities in male meiocytes, including chromosome fragmentation at anaphase I (Extended Data Fig. 3), suggesting that J3 is required for flowering, male gametogenesis, meiotic chromosome segregation and fertility. The hcr3 plants shared the late-flowering phenotype with j3 knockout alleles (all $P < 5.05 \times 10^{-9}$) but showed normal meiotic chromosome segregation, pollen and fertility (Extended Data Figs. 1i,j and 3). Interestingly, the hcr3 allele showed higher 420 crossover frequency (30 cM) than the j3 knockout alleles (25 cM) (Fig. 1b,d and Extended Data Fig. 2e), indicating that hcr3 is a dominant-negative allele of J3. Consistently, primary transgenic (T$_1$) plants expressing the J3^{G155R} allele under the J3, constitutive RPS5A (RIBOSOMAL PROTEIN 5A) or meiotic prophase I gene promoters in the Col background showed higher 420 and CTL5.14 crossover frequencies than Col and T$_1$ plants expressing J3 (all $P < 2.09 \times 10^{-3}$) (Fig. 1e–g and Supplementary Tables 6 and 7). Using SPO11-1::J3^{G155R} transgenic plants, we found that J3^{G155R} transcript levels correlate with CTL5.14 crossover frequencies ($R^2 = 0.84$, $P = 0.03$, $r = 0.91$) (Fig. 1g), demonstrating a dosage effect of J3^{G155R} expression in increasing crossover frequency.

J3^{G155R} dominantly inhibits J3 and J2

Arabidopsis encodes a J3 paralogue, J2 (At5g22060) (Supplementary Fig. 2). J3 and J2 proteins share 90% amino acid sequence identity, leading our anti-J3 to recognize both J3 and J2 proteins (Supplementary Fig. 2b,c and Extended Data Fig. 1f–h). RNA-seq analysis revealed that the transcript level of J3 is about fourfold higher than that of J2 in seedlings and flower buds (Extended Data Fig. 1c,e). Consistently, our immunoblot analysis using anti-J3 detected the remaining J2 proteins in j3-1 and j3-3, compared to Col (all $P < 1.36 \times 10^{-2}$) (Extended Data Fig. 1g,h). In contrast, we detected ~60–80% (in seedlings) to wild-type levels (in flower buds) of J3 proteins in j2-2, a T-DNA mutant that does not produce functional J2 transcripts, compared to the Col (Extended Data Fig. 1a–h). We observed that j2-2 exhibited normal crossover frequency, flowering time, pollen viability and fertility, suggesting that the more abundantly expressed J3 proteins function redundantly with J2 and compensate for their absence in j2-2 (Extended Data Figs. 1i,j and 3 and Supplementary Tables 4 and 8). Consistently, j3-1 j2-2/+ (25 cM) and j3/+ j2-2 (20 cM) plants showed the same 420 crossover frequency as j3-1 (25 cM) ($P = 0.78$) and j2-2 (20 cM) ($P = 0.58$) plants, respectively (Extended Data Fig. 2d and Supplementary Table 8), suggesting that the increased crossover frequency depends on j3-1. However, transgenic J3::J2^{G156R} plants expressing J2^{G156R} under the J3 promoter, mimicked the dominant-negative hcr3 allele, showing an increased 420 crossover frequency similar to hcr3 ($P = 4.23 \times 10^{-8}$) and transgenic T$_1$ plants expressing J2 in the j3-1 under the J3 promoter restored 420 crossover frequency to wild-type levels ($P = 0.74$) (Extended Data Fig. 2e and Supplementary Table 9). Furthermore, we observed that meiotic knockdown of J2 in the j3-1 background using meiosis-specific miRNA-induced gene silencing (meiMIGS) resulted in higher 420 crossover frequency than that in j3-1 ($P = 1.14 \times 10^{-4}$) (Extended Data Fig. 2e and Supplementary Table 9), demonstrating functional redundancy between J2 and J3 for crossover formation, with J3 playing a major role. Consistently, we also observed that j3-1 j2-2/+ and j3-1/+ j2-2 plants

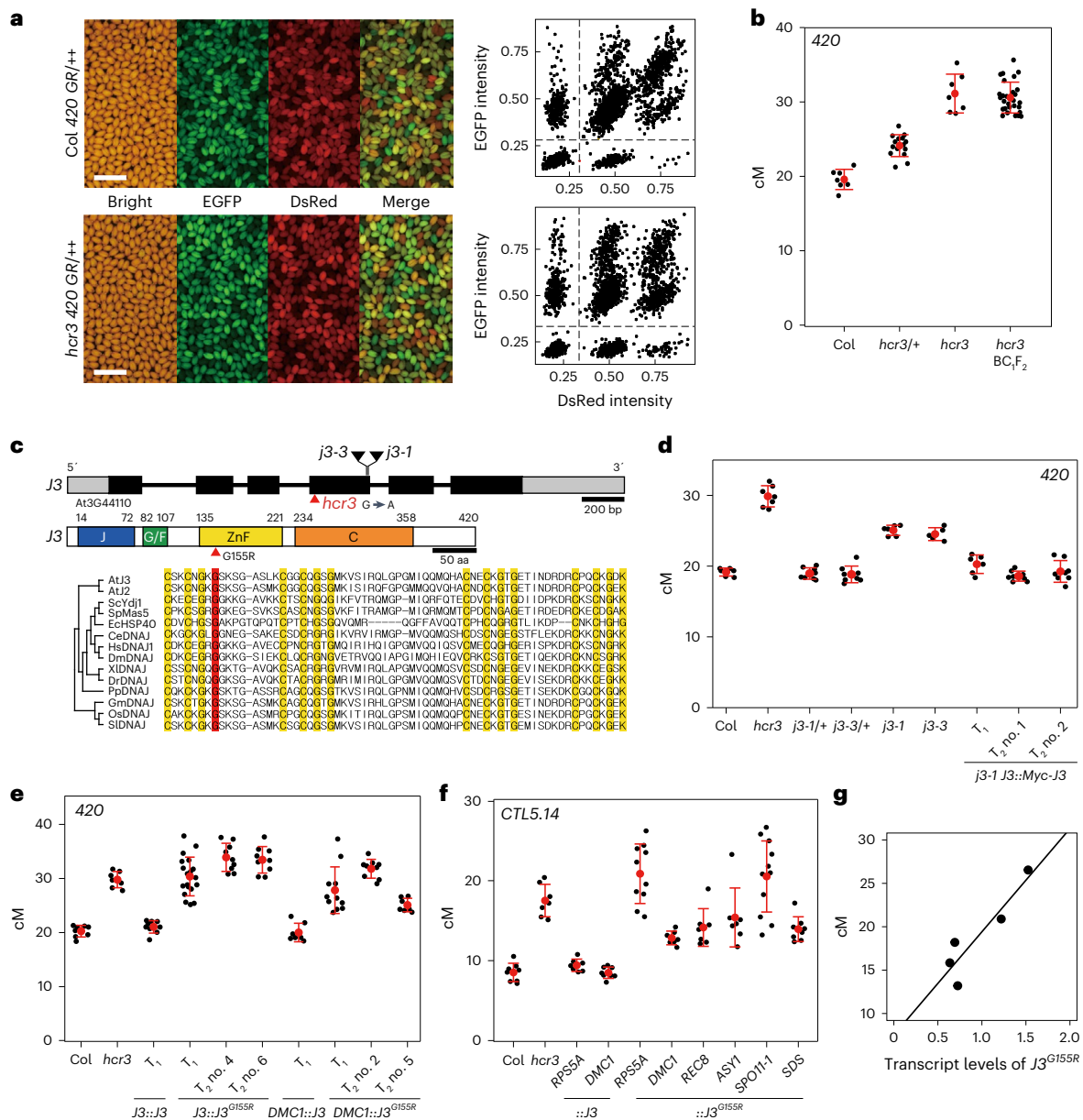**Fig. 1 | Isolation of *hcr3* as a dominant-negative *j3* mutant. a**, Representative images of fluorescent seed crossover reporter *420* in wild-type Col and *hcr3*. Scale bars, 2 mm. **b**, *420* crossover frequency (cM) in Col (*n* = 7), *hcr3/+* (*n* = 15), *hcr3* (*n* = 7) and *hcr3* BC$_1$F$_2$ (*n* = 28) plants. **c**, *hcr3* mutation and *J3* and J3 secondary structure. Exons are presented as boxes (black, coding sequence; grey, untranslated regions) and introns as lines. The red arrow indicates the G-to-A substitution site of *hcr3*. The ZnF regions of J3 orthologues from diverse eukaryotes are shown with a phylogenetic tree. **d**, *420* crossover frequency (cM) in Col (*n* = 6), *hcr3* (*n* = 7), *j3-1/+* (*n* = 8), *j3-3/+* (*n* = 11), *j3-1* (*n* = 6), *j3-3* (*n* = 5), *j3-1 J3::Myc-J3* T$_1$ (*n* = 6), *j3-1 J3::Myc-J3* T$_2$ no. 1 (*n* = 8) and *j3-1 J3::Myc-J3* T$_2$ no. 2 (*n* = 8) plants. **e**, As in **d** but showing transgenic plants expressing *J3^{G155R}*. Col (*n* = 8),

hcr3 (*n* = 7), *J3::J3* T$_1$ (*n* = 9), *J3::J3^{G155R}* T$_1$ (*n* = 19), *J3::J3^{G155R}* T$_2$ no. 4 (*n* = 9), *J3::J3^{G155R}* T$_2$ no. 6 (*n* = 9), *DMC1::J3* T$_1$ (*n* = 7), *DMC1::J3^{G155R}* T$_1$ (*n* = 11), *DMC1::J3^{G155R}* T$_1$ no. 2 (*n* = 9), *DMC1::J3^{G155R}* T$_1$ no. 5 (*n* = 7) plants. **f**, As in **e** but showing *CTL5.14* crossover frequencies using different meiotic gene promoters. Col (*n* = 7), *RPS5A::J3* T$_1$ (*n* = 7), *DMC1::J3* T$_1$ (*n* = 8), *RPS5A::J3^{G155R}* T$_1$ (*n* = 10), *DMC1::J3^{G155R}* T$_1$ (*n* = 6), *REC8::J3^{G155R}* T$_1$ (*n* = 7), *ASY1::J3^{G155R}* T$_1$ (*n* = 7), *SPO11-1::J3^{G155R}* T$_1$ (*n* = 12), *SDS::J3^{G155R}* T$_1$ (*n* = 8) plants. **g**, Correlation between crossover frequencies (cM) and *J3^{G155R}* transcript levels in *SPO11-1::J3^{G155R}* transgenic plants. **b**,**d**–**f**, Black dots indicate cM values of individual plants. Red dots and horizontal lines represent mean ± s.d. of cM values from individual plants (two-sided Welch's *t*-test). *n*, number of biologically independent plants.

exhibited more severe defects in pollen and seedling development compared to *j3-1* and *j2-2* single mutants, with ~5% of the progeny showing seedling lethality (Extended Data Fig. 3a–f). These results suggest that most *j3-1 j2-2* mutants result in pollen, embryo and seedling lethality, as described previously[37]. In addition, our yeast two-hybrid and co-immunoprecipitation assays revealed that the dominant-negative J3^{G155R} proteins form dimers with both J3 and J2 proteins (Extended Data Fig. 2f–h). Taken together, these results suggest that J3^{G155R} proteins produced by the *hcr3* allele increase crossovers in a dosage-dependent

manner by dimerizing with J3 and J2 proteins and dominantly inhibiting J3/J2-HSP70 chaperone network-mediated activity.

hcr3 increases crossovers in male and female meiosis

Next, we investigated the genome-wide effect of *hcr3* on crossover frequency using a set of recombination reporter CTLs/FTLs located in several genomic regions (Fig. 2a). Sixteen seed-CTLs and three pollen FTLs on distal chromosome regions showed higher crossover frequencies in *hcr3* than Col (all *P* < 2.18 × 10^{-3}), whereas three CTLs spanning

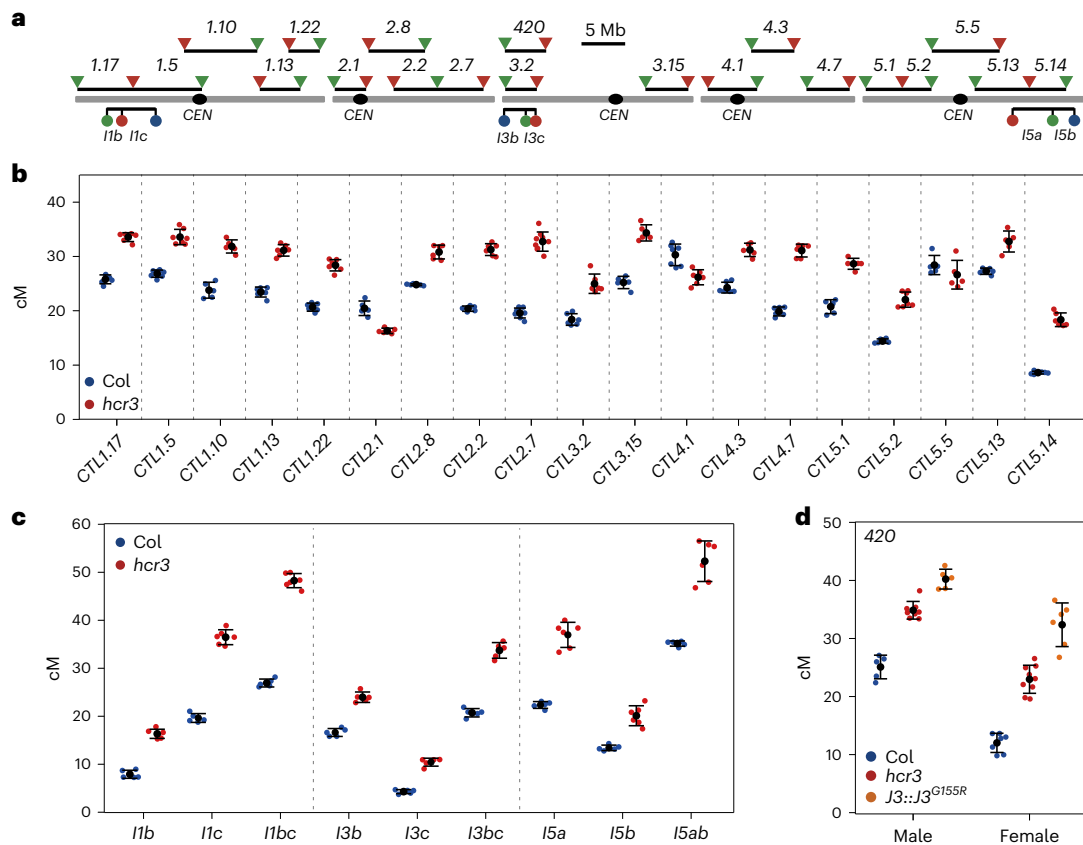**Fig. 2 | Increased crossover frequencies in chromosome arms in *hcr3* and *J3::J3^{G155R}* plants. a**, Seed (triangles) and pollen (circles) FTLs throughout the *Arabidopsis* genome. Lines represent the interval positions. **b**, Sex-averaged crossover frequencies of 19 seed FTLs/CTLs in Col (blue) and *hcr3* (red). *CTL1.17* Col ($n = 6$), *hcr3* ($n = 6$); *CTL1.5* Col ($n = 7$), *hcr3* ($n = 7$); *CTL1.10* Col ($n = 5$), *hcr3* ($n = 5$); *CTL1.13* Col ($n = 5$), *hcr3* ($n = 6$); *CTL1.22* Col ($n = 6$), *hcr3* ($n = 7$); *CTL2.1* Col ($n = 5$), *hcr3* ($n = 5$); *CTL2.8* Col ($n = 5$), *hcr3* ($n = 6$); *CTL2.2* Col ($n = 5$), *hcr3* ($n = 6$); *CTL2.7* Col ($n = 8$), *hcr3* ($n = 9$); *CTL3.2* Col ($n = 6$), *hcr3* ($n = 6$); *CTL3.15* Col ($n = 5$), *hcr3* ($n = 5$); *CTL4.1* Col ($n = 7$), *hcr3* ($n = 6$); *CTL4.3* Col ($n = 6$), *hcr3* ($n = 5$); *CTL4.7* Col ($n = 6$) *hcr3* ($n = 6$); *CTL5.1* Col ($n = 5$), *hcr3* ($n = 5$); *CTL5.2* Col ($n = 5$), *hcr3* ($n = 7$); *CTL5.5* Col ($n = 5$), *hcr3* ($n = 5$); *CTL5.13* Col ($n = 5$), *hcr3* ($n = 5$); *CTL5.14* Col ($n = 7$), *hcr3* ($n = 6$). **c**, As for **b** but showing male crossover frequencies of pollen FTLs. *I1b*, *I1c*, *I1bc* Col ($n = 5$), *hcr3* ($n = 6$); *I13b*, *I3c*, *I3bc* Col ($n = 5$), *hcr3* ($n = 5$); *I5a*, *I5b*, *I5ab* Col ($n = 5$), *hcr3* ($n = 6$). **d**, Sex-specific crossover frequencies of seed FTL *420* interval in Col (blue), *hcr3* (red) and *J3::J3^{G155R}* (orange) for male and female meiosis. Male Col ($n = 5$), *hcr3* ($n = 8$), *J3::J3^{G155R}* ($n = 5$); female Col ($n = 7$), *hcr3* ($n = 9$), *J3::J3^{G155R}* ($n = 6$). **b**–**d**, Blue, red and orange dots indicate cM values of individual plants. Mean ± s.d. of cM values from individual plants are indicated by black dots and horizontal lines (two-sided Welch's *t*-test). *n*, number of biologically independent plants.

centromeres showed unchanged or moderately reduced crossover frequency (*CTL2.1*, $P = 1.21 \times 10^{-3}$; *CTL4.1*, $P = 1.15 \times 10^{-3}$; *CTL5.5*, $P = 0.25$) (Fig. 2b,c and Supplementary Tables 10 and 11). This indicates that *hcr3* promotes crossovers within the chromosome arms but to a lesser extent within the pericentromeric and centromeric regions. To investigate the effect of HCR3 on male and female meiotic crossover recombination, we performed reciprocal crosses between *420 GR/++* Col, *hcr3* or *J3::J3^{G155R}* plants with Col. We observed that *hcr3* and *J3::J3^{G155R}* showed higher *420* crossover frequencies in both male and female meiosis compared to the Col (all $P < 4.24 \times 10^{-5}$) (Fig. 2d and Supplementary Table 12), demonstrating that HCR3 limits recombination in both male and female meiosis.

J3^{G155R} expression increases crossovers genome-wide

To investigate the effect of *J3^{G155R}/hcr3* allele on the genomic crossover landscape at high resolution, we performed genotyping-by-sequencing (GBS) of F_2 individuals from self-pollinated F_1 plants derived from a cross between a *J3::J3^{G155R}* Col transgenic line (T_1 no. 4) and the polymorphic Landsberg *erecta* (Ler) accession, as well as F_2 individuals from Col × Ler F_1 plants, which serves as a wild-type control (Extended Data Fig. 4a,b and Supplementary Table 13)[24,38,39]. *J3^{G155R}* led to around twice as many crossovers across the genome and on each chromosome in *J3::J3^{G155R}* Col × Ler F_2 individuals (T_1 no. 4, $n = 96$) compared

to Col × Ler F_2 plants ($n = 240$) (all $P < 9.43 \times 10^{-13}$) (Fig. 3a,b, Extended Data Fig. 4c,d and Supplementary Table 14). We also performed GBS of F_2 individuals of two independent *J3::J3^{G155R}* Col × Ler plants (T_1 no. 6, $n = 48$; T_1 no. 8, $n = 48$) and one *SPO11-1::J3^{G155R}* Col × Ler plant (T_1 no. 1, $n = 96$), which revealed that three independent *J3^{G155R}* transgenes elevated crossovers genome-wide by approximately twofold (all $P < 2.19 \times 10^{-5}$) (Extended Data Fig. 5 and Supplementary Tables 13 and 14). The additional crossovers occurred along the chromosome arms but were still suppressed around centromeres (Fig. 3b and Extended Data Figs. 4d and 5d,e), similar to the crossover frequency of CTLs analysed in *hcr3* (Fig. 2b–d). Sex-specific crossover maps from reciprocal crosses between *J3^{G155R}* Col × Ler F_1 and Ler revealed that *J3^{G155R}* increases crossover approximately twofold in both male and female meiosis (all $P < 1.30 \times 10^{-3}$) (Fig. 3c,d, Extended Data Fig. 4e,f and Supplementary Table 15), confirming that *J3^{G155R}* exerts the same effects on male and female crossovers.

We observed that *hcr3 fancm* and *hcr3 recq4a recq4b* mutants have higher *420* and *I3bc* crossover frequencies, respectively, compared to *hcr3*, *fancm* and *recq4a recq4b* (*recq4a/4b*) (all $P < 3.12 \times 10^{-4}$) (Fig. 4a,b and Supplementary Tables 17 and 18). *J3^{G155R}* also resulted in additively increased crossovers in *recq4a/4b* Col × Ler F_1 hybrid plants (all $P < 3.63 \times 10^{-3}$) (Fig. 3e,f, Extended Data Fig. 4g,h and Supplementary Table 16), which is similar to the combined effects of *HEI10*
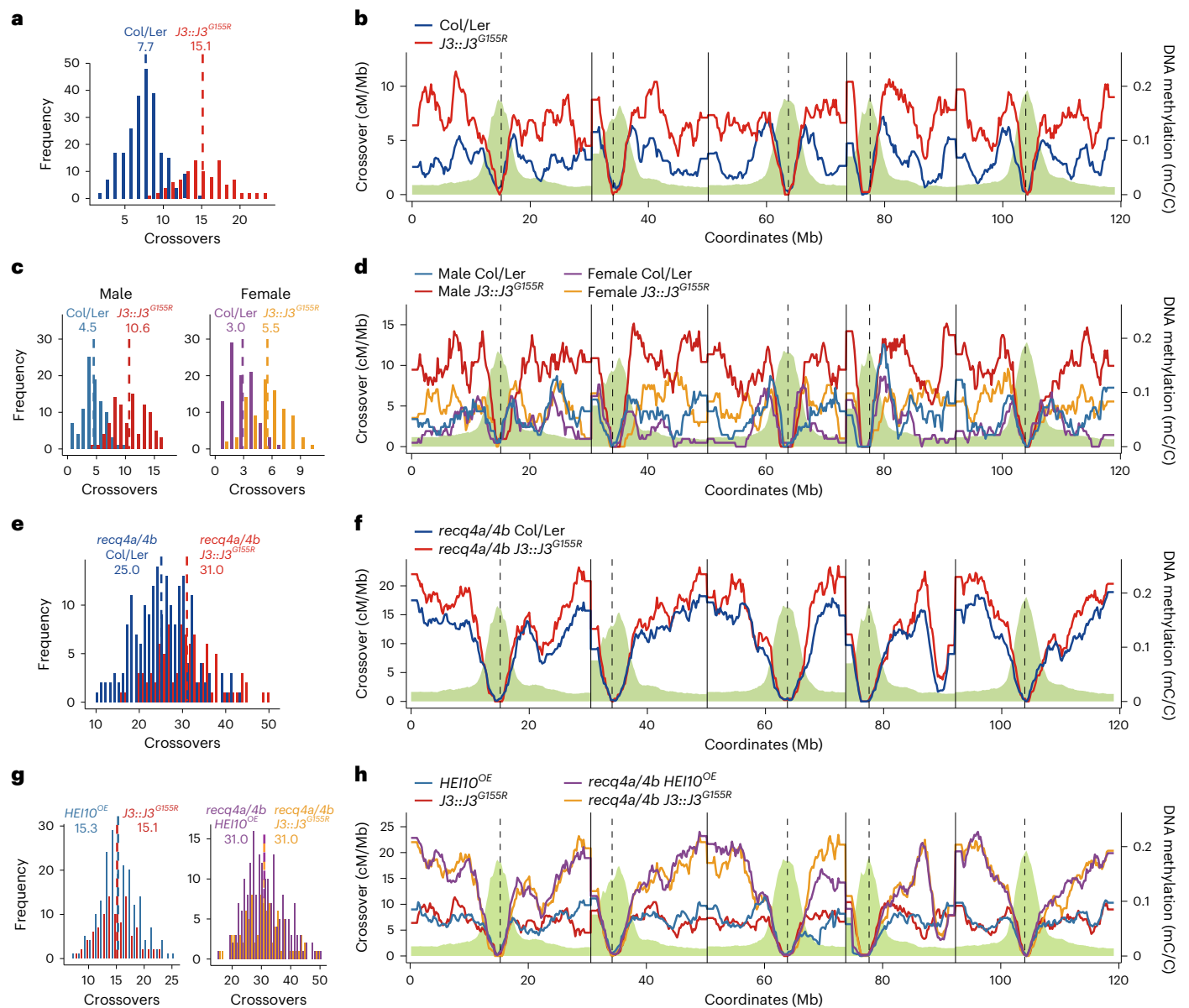
Fig. 3 | $J3^{G155R}$ expression increases crossovers in a hybrid context.
a,b, Histograms of sex-averaged crossover number (**a**) and genomic crossover landscapes (**b**) in Col × Ler (blue, $n = 240$) and $J3::J3^{G155R}$ Col × Ler (red, $n = 96$) F₂ individuals. **c,d**, As in **a,b** but showing analysis from male (blue, Col × Ler, $n = 96$; red, $J3^{G155R}$ Col × Ler, $n = 96$) and female (purple, Col × Ler, $n = 95$; orange, $J3::J3^{G155R}$ Col × Ler, $n = 90$) meiosis. **e,f**, As in **a,b** but showing analysis from a *recq4a recq4b* background (blue, *recq4a/4b* Col × Ler, $n = 151$; red, *recq4a/4b*

$J3::J3^{G155R}$ Col × Ler, $n = 96$). **g,h**, As in **a,b** but showing analysis from *HEI10^OE* (blue, $n = 192$), $J3::J3^{G155R}$ (red, $n = 96$), *recq4a/4b HEI10^OE* (purple, $n = 192$) and *recq4a/4b* $J3::J3^{G155R}$ (orange, $n = 96$). **a,c,e,g**, Significance between genotypes was tested by two-sided Welch's *t*-tests. **b,d,f,h**, Green indicates DNA methylation levels along chromosomes. Vertical solid and dashed lines represent telomeres and centromeres, respectively. n, the number of individual plants.

overexpression and *recq4a recq4b* mutations on crossover number and distribution (Fig. 3g,h)[15]. These results imply that HCR3 acts in parallel to the RECQ4A/4B and FANCM anti-crossover pathways and may restrict the HEI10-dependent class I crossovers.

To compare the effects of *j3* knockout and the $J3^{G155R}$ transgene on meiotic crossovers, we sought to map crossovers genome-wide in the *j3* knockout background using the GBS approach (Extended Data Fig. 6). To achieve this, we generated new *j3* null alleles of *j3-5*, *j3-6* and *j3-7* with premature stop codons in Ler background using CRISPR/Cas9 mutagenesis (Extended Data Fig. 6a). Like *j3-1* and *j3-3* in the Col background, the *j3-5* to *j3-7* alleles in Ler showed reduced pollen viability and fertility (all $P < 1.43 × 10^{-5}$) (Extended Data Fig. 6b–d). We observed that *420* crossover frequency was increased in *j3-1* Col × *j3-5* Ler F₁ hybrids, compared to wild-type and *j3* heterozygous Col/Ler

hybrids ($P = 1.19 × 10^{-7}$) (Extended Data Fig. 6e). Our genome-wide crossover mapping analysis of *j3-1* × *j3-5* F₂ individuals ($n = 96$) revealed that *j3* knockout increased the number of crossovers by ~30% on each chromosome (all $P < 1.98 × 10^{-2}$) and across the genome ($P = 2.08 × 10^{-9}$) compared to Col × Ler F₂ plants ($n = 240$) (Extended Data Fig. 6f–i). This suggests that expression of the $J3^{G155R}$ transgene inhibits both J3 and J2 proteins, thereby increasing crossovers more than *j3* knockout alone.

hcr3 increases class I crossovers and decreases interference
To gain further genetic insight into the effect of *hcr3* on class I and class II crossovers, we generated the *hcr3 hei10*, *hcr3 zip4* and *hcr3 mus81* double mutants (Fig. 4a,c). The *hcr3 hei10* and *hcr3 zip4* showed the same suppressed *420* crossover frequencies as *hei10* and *zip4* single mutants, indicating that the increased crossovers in *hcr3* are dependent
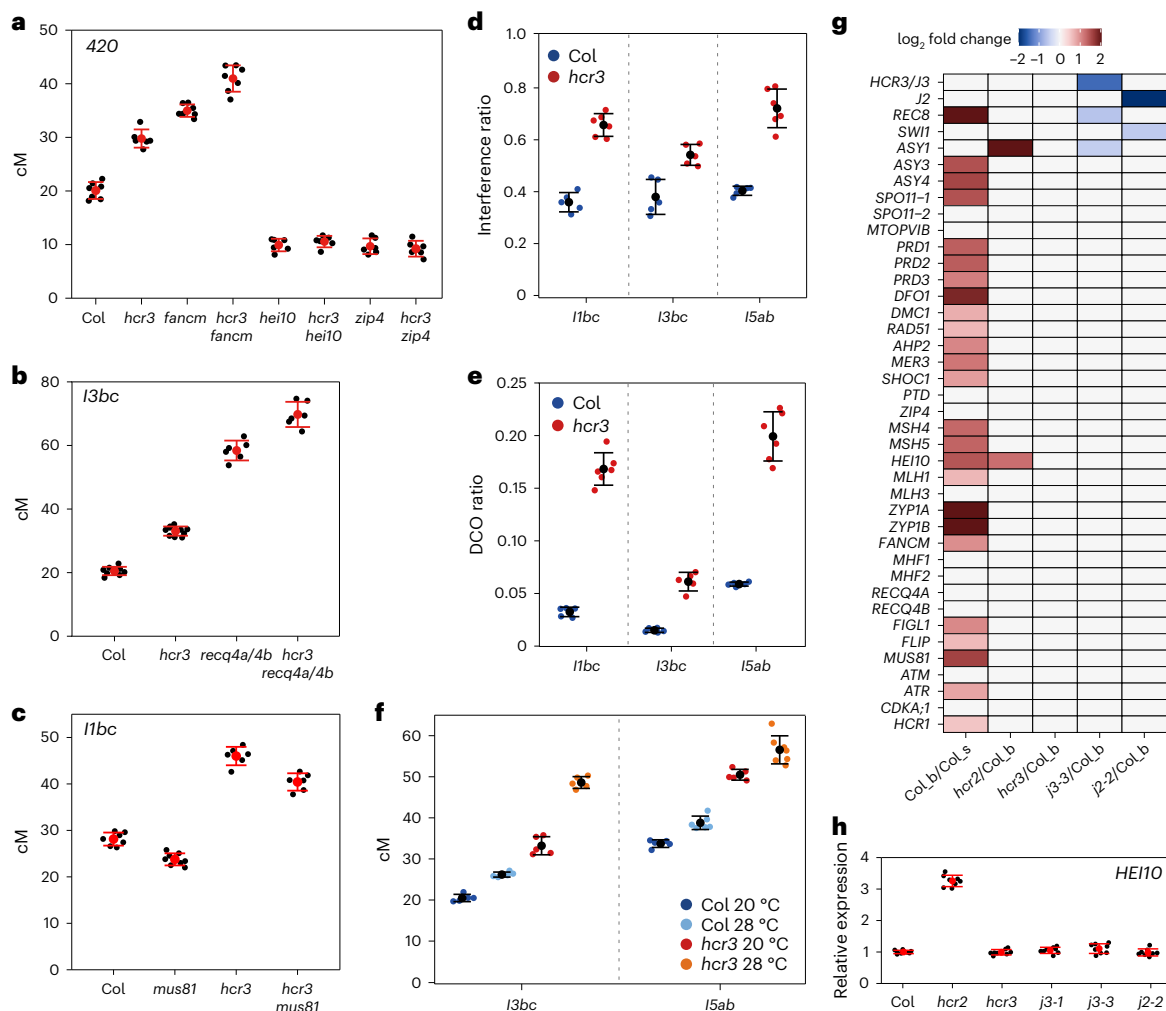
Fig. 4 | hcr3 increases interfering crossovers and reduces interference.
a, *420* crossover frequencies in Col (*n* = 7), *hcr3* (*n* = 6), *fancm* (*n* = 7), *hei10* (*n* = 6), *zip4* (*n* = 6) and combinations of *hcr3* in *fancm*, *hei10* and *zip4* (*hcr3 fancm n* = 7, *hcr3 hei10 n* = 6, *hcr3 zyp4 n* = 6). **b**, *I3bc* crossover frequencies in Col (*n* = 9), *hcr3* (*n* = 10), *recq4a recq4b* (*n* = 6) and *hcr3 recq4a recq4b* (*n* = 6). **c**, *I1bc* crossover frequencies in Col (*n* = 7), *mus81* (*n* = 8), *hcr3* (*n* = 6) and *hcr3 mus81* (*n* = 6). **d**,**e**, Crossover interference ratio (**d**) and double crossover (DCO) ratios (**e**) in FTL pollen tetrads in Col (blue) and *hcr3* (red). **f**, *I3bc* and *I5ab* crossover frequencies in Col and *hcr3* grown in optimal and high temperatures. *I3bc* Col 20 °C (*n* = 5), Col 28 °C (*n* = 5), *hcr3* 20 °C (*n* = 5), *hcr3* 28 °C (*n* = 5); *I5ab* Col 20 °C (*n* = 5), Col 28 °C (*n* = 6), *hcr3* 20 °C (*n* = 5), *hcr3* 28 °C (*n* = 7). **g**, Heatmap representation

of transcript levels and fold changes for meiotic recombination genes in Col seedlings (s), Col flower buds (b), *hcr2*, *hcr3*, *j3-3* and *j2-2* flower buds from RNA-seq data. **h**, RT–qPCR analysis of *HEI10* in Col, *hcr2*, *hcr3*, *j3-1*, *j3-3* and *j2-2* male meiocytes. Black dots indicate two technical duplicates of four biological replicates (*n* = 8 for each genotype) for RT–qPCRs. Red dots and horizontal lines indicate mean ± s.d. values of data points (two-sided Welch's *t*-test). Red (**a**,**b**,**c**) or black (**d**,**e**,**f**) dots and horizontal lines indicate mean ± s.d. of cM values from individual plants (two-sided Welch's *t*-test). Black (**a**,**b**,**c**) and coloured (**d**,**e**,**f**) dots represent cM values of individual plants. **a**–**f**, *n* is the number of biologically independent plants.

on HEI10 and ZIP4 (Fig. 4a and Supplementary Table 17). In contrast, *hcr3 mus81* showed an ~12.1% reduction in *I1bc* crossover frequency compared to *hcr3*, as *mus81* showed an ~15.5% reduction compared to Col (Fig. 4c and Supplementary Table 19). These genetic results demonstrate that HCR3 predominantly restricts interfering crossovers.

To determine the effect of *hcr3* on interference, we measured the crossover interference ratio (IFR) using three-colour pollen FTLs (*I1bc*, *I3bc* and *I5ab*), which allow mapping genetic distance of a test interval with and without a crossover in the adjacent interval[24,40]. The interference ratios increased as the incidence of double crossovers increased in *hcr3*, compared to Col (all *P* < 2.55 × 10⁻³) (Fig. 4d,e and Supplementary Table 11), indicating that interference strength is decreased in *hcr3* but not completely abolished. Interfering crossovers in *Arabidopsis* are sensitive to changes in ambient temperature, showing a moderate increase at higher temperature (28 °C), compared to an optimal growth temperature (18–20 °C)[41,42]. We observed that *hcr3* showed higher crossover frequencies in *I3bc* and *I5ab* at both optimal and higher

temperatures than Col (Fig. 4f and Supplementary Table 20), again supporting that HCR3 inhibits formation of interfering crossovers.

hcr3 and *j3* increase the numbers of MLH1 foci per meiocyte
Because the additional crossovers in *hcr3* depend on HEI10 (Fig. 4a)[11,15], we performed transcriptomic (RNA-seq) analysis in Col, *hcr3*, *j3-3* and *j2-2* flower buds to examine whether *hcr3* and *j3* affect *HEI10* transcription. The transcript levels of *HEI10* were not altered in *hcr3*, *j3-3* or *j2-2* but were increased in *hcr2*, as observed previously[38] (Fig. 4g). To confirm the effects of *hcr3* and *j3* on *HEI10* transcription during meiosis, we purified male meiocytes and performed quantitative PCR with reverse transcription (RT–qPCR) analysis. Again, we observed that *HEI10* transcript levels were not changed in *hcr3*, *j3-1*, *j3-3* and *j2-2* compared to Col (*t*-test, all *P* > 0.1) but were increased in *hcr2* (*P* = 4.34 × 10⁻¹⁰) (Fig. 4h). Cytological analysis showed that meiotic axis formation, synapsis, chromosome segregation and pollen viability are normal in *hcr3* (Extended Data Fig. 3a,b,f, Supplementary Fig. 4a

and Supplementary Table 21). The DNA double-strand break marker, RAD51, remained unchanged in *hcr3* male meiocytes (Wilcoxon test, $P = 0.4$) (Supplementary Fig. 4b,c and Supplementary Table 22) but the number of MLH1 foci, a marker of class I crossover sites, increased in *hcr3* compared to Col at late-pachytene, diplotene and diakinesis (Wilcoxon test, all $P < 1.23 \times 10^{-4}$) (Fig. 5a,b and Supplementary Table 23). Similar to *hcr3*, we also observed an increase in the number of MLH1 foci per cell in *j3-1* and *j3-3* (Wilcoxon test, *j3-1* $P = 1.15 \times 10^{-2}$, *j3-3* $P = 5.88 \times 10^{-3}$) (Extended Data Fig. 6j and Supplementary Table 23), demonstrating that HCR3 restricts interfering crossovers.

HEI10 foci are increased and more closely spaced in *hcr3*

Increased MLH1-immunostaining is consistent with *hcr3* increasing the abundance of HEI10 or other ZMM factors. Therefore, we quantified immunostained foci for HEI10 in *hcr3* using super-resolution structured illumination microscopy with co-immunostaining for ZYP1, a marker of the SC (Fig. 5c,d)[18]. We observed an increase in the number of late-pachytene HEI10 foci per bivalent in *hcr3* (Wilcoxon test, $P < 5.97 \times 10^{-7}$) (Fig. 5c,d). Moreover, the distance between adjacent HEI10 foci along chromosome axes decreased, with a high coincidence of closely spaced HEI10 foci in *hcr3* (mean = 16.7 μm), compared to the Col (mean = 23.0 μm, Wilcoxon test, $P < 2.64 \times 10^{-7}$) (Fig. 5d). Because our recent HEI10 coarsening model can explain the effects of HEI10 expression levels on crossover number and interference[18], we tested whether the effect of *hcr3* on HEI10 foci is consistent with this model. We ran simulations using the same parameter values from ref. 18 and *hcr3* simulations, which were identical to Col simulations but with 1.3× the initial amount of HEI10 along the SC and at recombination intermediate sites. The *hcr3* simulation outputs showed an increased number and closer spacing of crossovers compared to Col simulations (Wilcoxon test, all $P < 2.20 \times 10^{-16}$) (Fig. 5d)[18]. However, we note that closely spaced HEI10 foci were over-represented in *hcr3* experimental data compared to crossovers in *hcr3* simulations. This suggests that the effects of *hcr3* on crossovers are, at least in part, mediated by changes in HEI10 abundance and/or dynamics. Correspondingly, male- and female-specific crossover maps revealed that *J3::J3^G155R* Col × Ler F$_1$ plants show more crossovers and shorter physical distances between crossovers on the same chromosomes (male mean = 7.7 Mb, female mean = 10.0 Mb) compared to Col × Ler F$_1$ plants (male mean = 11.4 Mb, female mean = 13.3 Mb, Wilcoxon test, all $P < 1.00 \times 10^{-2}$) (Figs. 3c,d and 5e, Extended Data Fig. 4e,f and Supplementary Table 24). Notably, as in wild-type Col × Ler F$_1$ plants, the crossovers in *J3::J3^G155R* Col × Ler F$_1$ plants were more widely spaced than expected from a random distribution (Wilcoxon test, *J3^G155R*, all $P < 9.70 \times 10^{-6}$), indicating that *J3^G155R* reduces but does not eliminate crossover interference (Fig. 5e and Supplementary Table 24), consistent with *hcr3* decreasing interference in pollen tetrad analysis (Fig. 4d,e).

HCR3 interacts with HEI10 on the synaptonemal complex

By co-immunostaining for J3, ASY1, ZYP1 and DNA during meiosis, we found that both J3 and J3^G155R signals localize to the nucleus, surrounding the axis (ASY1) and transverse elements (ZYP1) of the SC signals at leptotene, zygotene and pachytene stages in Col and *hcr3*, with weak signals for the remaining J2 proteins in *j3-1* (Fig. 6a and Supplementary Fig. 4d). These results prompted us to investigate whether the J3 co-chaperone interacts with meiotic recombination proteins using

yeast two-hybrid assays. Indeed, both J3 and J3^G155R interacted strongly with HEI10, PTD, MSH5 and ZIP4 and weakly with MER3 but not with SHOC1 or MLH1 (Fig. 6b and Supplementary Table 25). We also detected an interaction between J3 and J3^G155R with other meiotic proteins such as ASY1, an axis element of SC, indicating that J3 is a broad protein partner, as expected for class A HSP40 co-chaperones (Supplementary Table 25)[33]. We confirmed the protein interactions of J3 and J3^G155R with HEI10, PTD and MSH5 in planta using co-immunoprecipitation and TurboID-based proximity labelling assays in *Arabidopsis* protoplasts (Supplementary Fig. 5).

To investigate the interactions of J3 and J3^G155R with HEI10 at recombination intermediates in vivo, we performed co-immunostaining of J3, J3^G155R and HEI10, along with ZYP1, during pachytene in wild-type and *hcr3* male meiocytes (Fig. 6c). We observed that most immunostained signals of small and large HEI10 foci at recombination intermediates co-localized with the signals of J3/J2 in Col and J3^G155R/ J2 in *hcr3* at the mid-pachytene stage (Fig. 6c). Furthermore, our co-immunofluorescence analysis of pollen mother cells using epitope HA and Myc antibodies confirmed the co-localization of distinct HEI10-Myc foci with HA-J3 and HA-J3^G155R at late-pachytene stages in *HEI10::HEI10-Myc*, *HEI10::HEI10-Myc hcr3*, *J3::-HA-J3 HEI10::HEI10-Myc* and *J3:HA-J3^G155R HEI10::HEI10-Myc* plants (Extended Data Fig. 7a,c). We also observed that immunostained J3 signals co-localize with HEI10-Myc foci at diplotene and diakinesis in *HEI10::HEI10-Myc* plants (Extended Data Fig. 7b). The co-localization of J3 and HEI10 foci at mid- to late-pachytene, diplotene and diakinesis stages suggest that J3 may interact with dynamic HEI10 foci at recombination intermediate sites, developing crossover sites and designated crossover sites.

HCR3 promotes degradation of HEI10 and pro-crossover factors

Because a J3 homologue, Ydj1, is required for protein degradation in budding yeast[34,43], we examined the effects of the *hcr3* and *j3-1* on protein turnover of HCR3-interacting ZMM proteins. We determined that HEI10, PTD and MSH5 were more abundant in *hcr3* and *j3-1* than in Col when their encoding constructs were transiently expressed in protoplasts (all $P < 1.89 \times 10^{-2}$) (Fig. 7a,b). Consistently, we detected higher protein levels of HEI10-Myc, PTD-Myc and MSH5-Myc in transgenic plants co-expressing *HA-J3^G155R*, compared to transgenic plants co-expressing *HA-J3* (HEI10-Myc $P = 4.47 \times 10^{-2}$, PTD-Myc $P = 1.17 \times 10^{-2}$, MHS5-Myc $P = 2.08 \times 10^{-3}$) (Fig. 7c,d). To investigate more direct effects of J3 and J3^G155R on HEI10 abundance, we transiently co-expressed Myc-J3 or Myc-J3^G155R with HEI10-HA in *j3-1* protoplasts and then quantified HEI10 abundance by immunoblot analysis (Fig. 7e,f). We observed that transiently expressed Myc-J3 proteins led to decreased HEI10-HA levels in *j3-1* protoplasts, compared to empty vector transfections ($P = 9.74 \times 10^{-3}$) and Myc-J3^G155R proteins maintained HEI10-HA levels in *j3-1* ($P = 3.02 \times 10^{-3}$) (Fig. 7e,f), indicating that J3 facilitates HEI10 degradation. More importantly, immunoblot analysis using anti-HEI10 showed that endogenous HEI10 protein abundance is higher in *j3-1*, *hcr3* and *J3::J3^G155R* transgenic plants than in Col (all $P < 4.70 \times 10^{-2}$) (Fig. 7g,h). These results suggest that HCR3 facilitates proteolysis of HEI10, PTD and MSH5 and that the additional crossovers in *j3-1*, *hcr3* and *J3::J3^G155R* plants are dependent on increased HEI10 abundance. Moreover, the effects of *hcr3* on crossover number

Fig. 5 | *hcr3* elevates interfering crossovers and closely spaced crossovers per bivalent. a, Representative images of immunostained MLH1 foci at diakinesis stage in three-dimensional preserved Col and *hcr3* male meiocytes. Nuclear DNA was stained with DAPI (white). Scale bars, 5 μm. **b**, Quantification of immunostained MLH1 foci at pachytene, diplotene and diakinesis stages in Col and *hcr3*. Each coloured dot indicates an individual cell of male meiocytes. Black dot and horizontal lines indicate mean ± s.d. values (two-sided Wilcoxon test). *n*, the number of biological independent cells. **c**, Representative images

of immunostained HEI10 foci and ZYP1 in Col and *hcr3* at late-pachytene stage. Scale bar, 5 μm. **d**, Comparison of late-pachytene cytological data and coarsening model simulation output showing the number of crossovers per bivalent and the distribution of spacing between adjacent crossovers in Col and *hcr3*. **e**, GBS analysis of plots showing the number of crossovers and inter-crossover distance per chromatid in Col × Ler and *J3::J3^G155R* Col × Ler F$_1$ hybrid male and female meiosis.
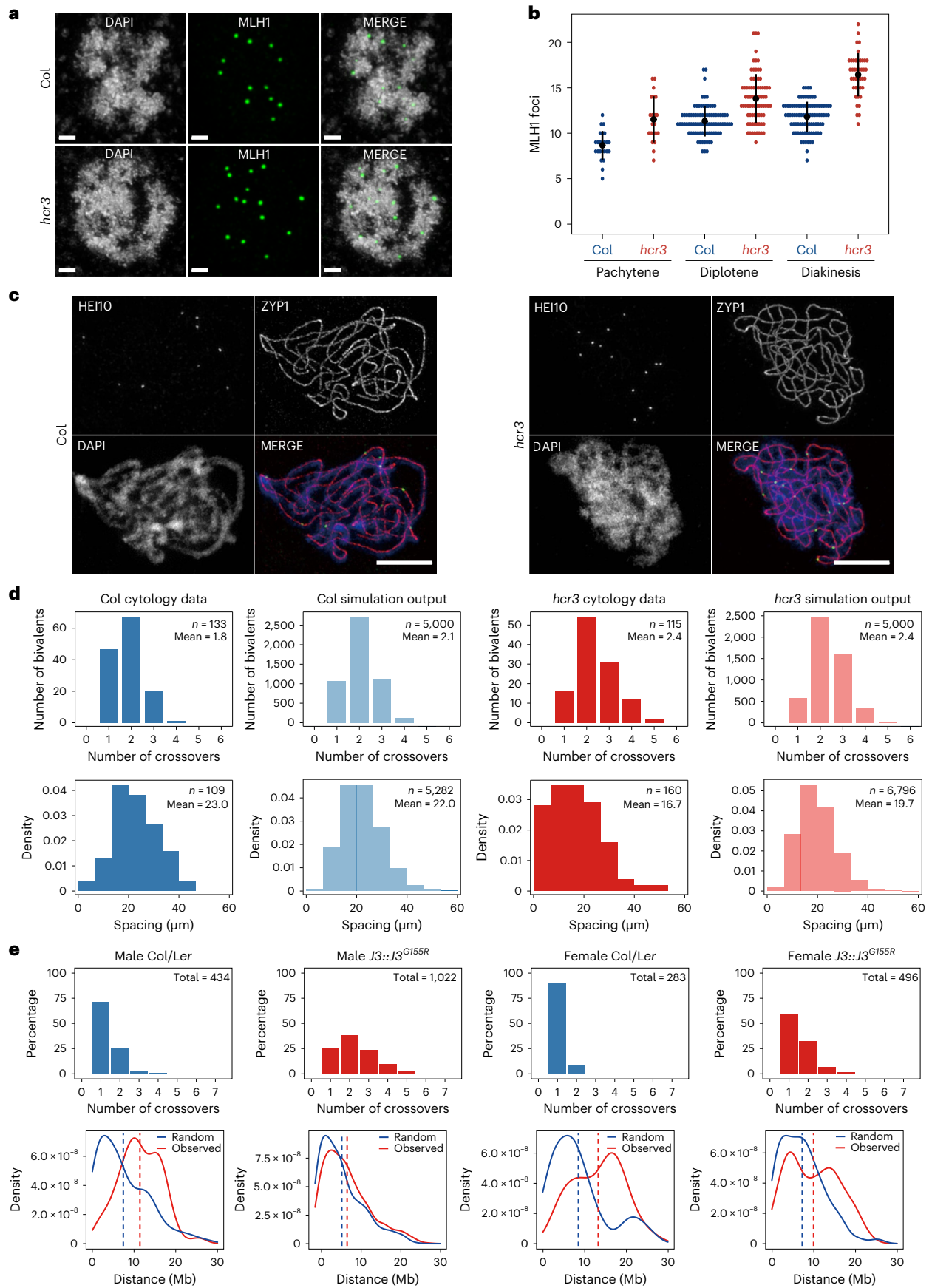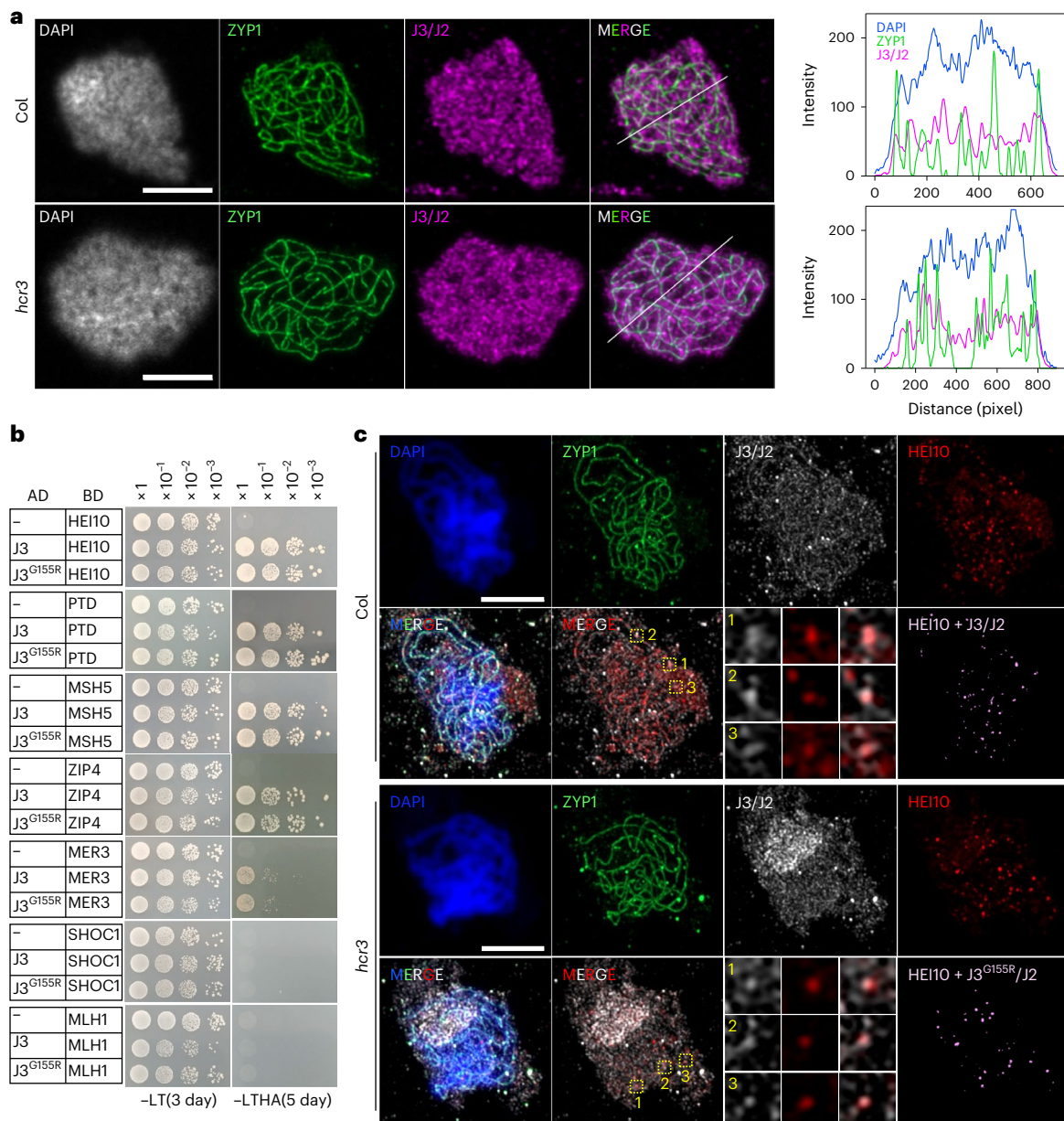
Fig. 6 | J3 interacts with ZMMs and co-localizes with HEI10. a, Representative images and signal intensity plots of co-immunostained J3/J2 (magenta) and ZYP1 (green) at the pachytene stage in wild-type Col and *hcr3*. Nuclear DNA was stained with DAPI (white in images, blue in plots). Representative bisecting white lines in merged images show plot profiles of intensities and positions for DAPI (blue), ZYP1 (green) and J3/J2 (magenta). Pixel of *x*-axis unit indicates 0.013 μm. Scale bars, 5 μm. **b**, Yeast two-hybrid assay showing the interaction of J3 and J3^{G155R} with ZMM proteins. **c**, Representative images of co-immunostained J3/J2 (white), ZYP1 (green) and HEI10 (red) at mid-pachytene stage in wild-type Col and *hcr3*. Three yellow dot boxes (1, 2, 3) in merged images of co-immunostained J3/J2 and HEI10 are enlarged and shown. Scale bars, 5 μm.

and, to a lesser extent, on crossover interference through the increased HEI10 abundance are consistent with the HEI10-mediated coarsening model (Fig. 5c,d)[18].

HCR3–HSP70 chaperone network facilitates HEI10 degradation

HSP40/J-protein dimers deliver specific substrates to HSP70 and interact with HSP70 through their J domain, synergistically promoting HSP70 ATPase activity[32]. Consistently, we detected physical interaction of HCR3 and J3^{G155R} with HSP70 in vitro and found that HCR3–HSP70 chaperones co-localize with HEI10, PTD and MSH5 in the nucleus of protoplasts co-transfected with their encoding constructs (Extended Data Fig. 8a,b,d). We also found that J2 interacts with HSP70 and HEI10 in co-immunoprecipitation and co-localization analyses (Extended Data

Fig. 8c,d). Therefore, we investigated the role of *Arabidopsis* HSP70 in crossover formation by meiotic knockdown of *HSP70* genes using meiMIGS (Extended Data Fig. 8e–k)[24,38,44]. We observed higher crossover frequencies in the *420, CTL1.17, CTL1.22, CTL3.15* and *CTL4.7* reporters (all $P < 6.91 \times 10^{-6}$) and higher HEI10 abundance in *meiMIGS-HSP70* transgenic plants than in the Col ($P = 1.23 \times 10^{-2}$), concomitantly with lower transcript levels of nuclear *HSP70* genes (all $P < 3.52 \times 10^{-2}$) (Fig. 7i,j, Extended Data Fig. 8e–i and Supplementary Table 26). In addition, we mapped crossovers genome-wide using GBS of *meiMIGS-HSP70* Col/Ler F$_2$ individuals (T$_1$ no. 1, $n = 96$) (Extended Data Fig. 8j,k), which revealed that *meiMIGS-HSP70* resulted in an increase in the number of crossovers (8.92/F$_2$) across the genome compared to controls ($P = 8.43 \times 10^{-5}$) (Extended Data Fig. 8j,k), suggesting that HSP70 and J3/J2 cooperate to restrict crossovers.

Because HSP40–HSP70 chaperones target protein aggregates or biomolecular condensates to other co-chaperones, such as HSP100 (*Arabidopsis* HSP101) and HSP90, for degradation by cooperating with the ubiquitin-proteasome system[32,45], we examined the effect of the *hsp101* mutation on HEI10 abundance using immunoblot analysis. We observed that *hsp101* did not increase HEI10 abundance (*P* = 0.75), crossover frequency (all *P* > 0.22) or MLH1 foci (Wilcoxon test, *P* = 0.93), compared to wild-type controls (Supplementary Fig. 6), suggesting that the HCR3–HSP70 chaperone network may facilitate HEI10 degradation and limit crossovers, potentially by cooperating with other co-chaperone machines such as HSP90.

HCR3 mediates ubiquitin and SUMO modifications of HEI10

To investigate how HCR3 mediates the protein turnover of HEI10, we examined the effect of *hcr3* on ubiquitin (Ub) and SUMO modifications of HEI10 using *HEI10::HEI10-Myc* and *hcr3 HEI10::HEI10-Myc* plants (Fig. 7k,l). Immunoprecipitation of HEI10-Myc and subsequent immunoblot analysis using Ub and SUMO antibodies revealed that HEI10 is modified by both ubiquitination and SUMOylation (Fig. 7k,l). Using anti-Ub specific for lysine 48 residue-linked Ub chains (K48-Ub) that triggers poly-ubiquitination-dependent proteasomal degradation, we observed lower levels of poly-Ub-conjugated HEI10-Myc proteins in *hcr3* than in the Col, when the intensities of poly-ubiquitylated HEI10-Myc proteins were normalized by those of immunoprecipitated and unmodified HEI10-Myc proteins (*P* = 2.85 × 10⁻³) (Fig. 7k,l). This result suggests that HCR3 promotes proteasomal degradation of HEI10 by facilitating its poly-ubiquitination. To further investigate ubiquitin-proteasome-dependent HEI10 degradation, we used the *Arabidopsis* protoplast transient expression system (Extended Data Fig. 9). In this system we transiently expressed either FLAG-tagged Ub (FLAG-Ub) or HEI10-HA or both, for immunoprecipitation and immunoblot analysis of HEI10-HA. We detected shifted bands indicative of FLAG-Ub-conjugated HEI10-HA proteins when FLAG-Ub and HEI10-HA were co-expressed, which were not evident in controls (Extended Data Fig. 9a), suggesting that ubiquitin modification of HEI10-HA may be mediated by a ubiquitin E3 ligase and/or HEI10-HA itself. HEI10-HA proteins underwent rapid degradation in protoplasts since translation elongation was blocked by the treatment with cycloheximide. However, HEI10-HA degradation was delayed and FLAG-Ub-conjugated HEI10-HA forms were increased upon treatment with the proteasome inhibitor MG132 (all *P* < 4.48 × 10⁻²) (Extended Data Fig. 9a–c), indicating that HEI10 degradation depends on the ubiquitin-proteasome system. Using anti-SUMO1 that recognizes SUMOylation in *Arabidopsis*, we also observed that poly-SUMOylated HEI10-Myc levels were decreased in *hcr3*, compared to the wild type (*P* = 3.05 × 10⁻²) (Fig. 7k,l), suggesting that poly-SUMOylation may also mediate HEI10 degradation. Taken together, we propose that HCR3 facilitates poly-Ub and poly-SUMO modifications of HEI10 that promote its degradation.

Discussion

Formation of protein aggregates or biomolecular condensates is counteracted by HSP40–HSP70 disaggregation chaperones and proteasomes for dispersal and degradation[19,32,35,45,46]. Our findings suggest that the disaggregating machinery facilitates proteolysis of HEI10- and HCR3-interacting ZMMs at recombination intermediate foci and SC to limit interfering crossovers during *Arabidopsis* meiosis (Fig. 7m). The HEI10/ZIP3 E3 ligase family is involved in the SUMO-ubiquitin-proteasome relay for crossover control in mouse and budding yeast[25,31]. Mammalian genomes encode both a SUMO E3 ligase (RNF212) and a ubiquitin E3 ligase (HEI10) that function to control crossovers[12,13]. The RNF212–HEI10 pathway stabilizes a minority of crossover-designated recombination intermediates through RNF212 and destabilizes most recombination intermediates through HEI10 for non-crossovers[12,13,31]. However, plants and the fungus *Sordaria* encode only the HEI10 family, while budding yeast and worms have only the ZIP3 family[4,9,10,14,16], suggesting a temporal or SUMO/ubiquitin switch activity of each family for selective stability and disruption of recombination intermediates. Our observations of ubiquitylated and SUMOylated HEI10 in the wild type and *hcr3* suggest that the HCR3–HSP70 chaperone network promotes HEI10 turnover and dynamics by facilitating both poly-ubiquitination and poly-SUMOylation of HEI10 via HEI10 autoregulation and/or other E3 ligases. As HEI10 dosage and diffusion-mediated coarsening determine crossover patterning in *Arabidopsis*[11,18], we propose that HCR3 co-chaperone molecules monitor the molecular status of HEI10 and growing HEI10-containing recombination foci for their disaggregation and degradation.

By increasing HEI10 abundance with our mathematical coarsening simulations, we were able to recapitulate experimental increases in HEI10 focus number in *hcr3*, supporting a coarsening-driven explanation for crossover patterning. Increased HEI10 abundance leads to more crossovers within the model by enabling more large HEI10 foci to stably persist until the end of prophase I[18]. In *hcr3*, increased HEI10 abundance at recombination intermediate sites and along the SC would result from a lack of HCR3-mediated HEI10 proteolysis. HCR3-mediated proteolysis is presumably required to stringently maintain specific HEI10 protein levels and, thus, preserve wild-type level of crossovers. This is supported by our immunoblot and cytological analyses of HEI10 abundance and positioning in *hcr3*. We also observed an increase in closely spaced HEI10 foci within our *hcr3* model, consistent with reduced crossover interference, although we note that closely spaced HEI10 foci were over-represented in our experimental data compared with our model, suggesting that HCR3 may also play a role in modulating other coarsening parameters. For example, it is possible that HCR3–HSP70 chaperone activities, such as substrate unfolding and folding, contribute to the disassembly or recycling dynamics of HEI10 foci at non-crossover and developing crossover sites, which allow diffusible HEI10 molecules to be remobilized to designated crossover sites. It will be intriguing to explore, using live imaging approaches[47], how the growing HEI10 foci are degraded and/or disaggregated at most recombination intermediates via the HCR3–HSP70 chaperone network, with only a subset further stabilized at designated crossover sites.

Our findings on HCR3 provide more evidence that HEI10 is a major target of anti-crossover factors, such as HCR1 and HCR2 in the class I pathway[24,38]. We determined that the *hcr1 hcr3* mutant has higher HEI10

Fig. 7 | HCR3 mediates proteolysis of HEI10. a,b, Immunoblot (**a**) and quantification (**b**) analyses of epitope-tagged HEI10, PTD, MSH5 and J3 in Col, *hcr3* and *j3-1* protoplasts. HEI10-HA, Col (*n* = 4), *hcr3* (*n* = 4), *j3-1* (*n* = 4); PTD-HA, Col (*n* = 6), *hcr3* (*n* = 6), *j3-1* (*n* = 6); MSH5-HA, Col (*n* = 6), *hcr3* (*n* = 6), *j3-1* (*n* = 6). **c,d**, Immunoblot (**c**) and quantification (**d**) analyses of epitope-tagged HEI10, PTD and MSH5 in flower buds of plants co-expressing *HA-J3* or *HA-J3^GI55R^*. HEI10-Myc, *HA-J3* (*n* = 3), *HA-J3^GI55R^* (*n* = 3); PTD-Myc, *HA-J3* (*n* = 3), *HA-J3^GI55R^* (*n* = 3); MSH5-Myc, *HA-J3* (*n* = 3), *HA-J3^GI55R^* (*n* = 3). **e,f**, As for **a,b** but showing epitope-tagged HEI10, J3 and J3^GI55R^ in *j3-1* protoplasts. HEI10-HA, *J3* (*n* = 7), *J3^GI55R^* (*n* = 6), empty vector (*n* = 5). Transcript levels of mRNA (**a,c,e**) were shown and used to calculate relative protein intensities (**b,d,f**). **g,h**, Immunoblot (**g**) and quantification (**h**) analyses of HEI10 in Col (*n* = 6), *hcr3* (*n* = 6), *j3-1* (*n* = 6) and *J3::J3^GI55R^* (*n* = 5). **i,j**, As for **g**

and **h** but showing in Col (*n* = 3) and *meiMIGS-HSP70-1* (*n* = 3) plants. **k,l**, Co-immunoprecipitation and followed by immunoblot (**k**) and quantification (**l**) analysis of ubiquitin- and SUMO-conjugated HEI10-Myc in Col *HEI10::HEI10-Myc* and *hcr3 HEI10::HEI10-Myc* plants. IP, immunoprecipitation; IB, immunoblot. K48-Ub, Col (*n* = 9), *hcr3* (*n* = 9); SUMO, Col (*n* = 3), *hcr3* (*n* = 3). Coloured (**b,d,l**) or black (**f,h,j**) dots represent the normalized intensities of immunoblot replicates. Black (**b,d,l**) or red (**f,h,j**) dots and horizontal lines indicate mean ± s.d. of normalized intensities of immunoblot replicates (two-sided Welch's test). Coomassie blue (CB)-stained (**a,e,g,i**) or Ponceau S-stained (**c,k**) membrane served as a loading control. *n*, the number of independent experiments. **m**, A model for the role of the HCR3–HSP70 chaperone network in limiting crossovers by promoting HEI10 degradation at recombination intermediate and designated crossover sites.

abundance and crossover frequency than each of the single mutants (Extended Data Fig. 10a,b and Supplementary Table 27), consistent with HEI10 being posttranslationally regulated in parallel by HCR1-catalysed dephosphorylation and chaperone-mediated proteolysis. It is likely that during HEI10 coarsening[18,48,49], HCR1 phosphatase and its counteracting kinases determine phosphorylation status of HEI10 (ref. 24).

Simultaneously, HCR3 may monitor the phosphorylation and conformational states of HEI10, facilitating its modification through ubiquitination and SUMOylation to promote degradation. Hence, we propose that the tight regulation of HEI10 abundance is required to mediate crossover interference and inhibit close-spacing of crossovers that are sensitive to changes in temperature and genome ploidy[41,42,50].
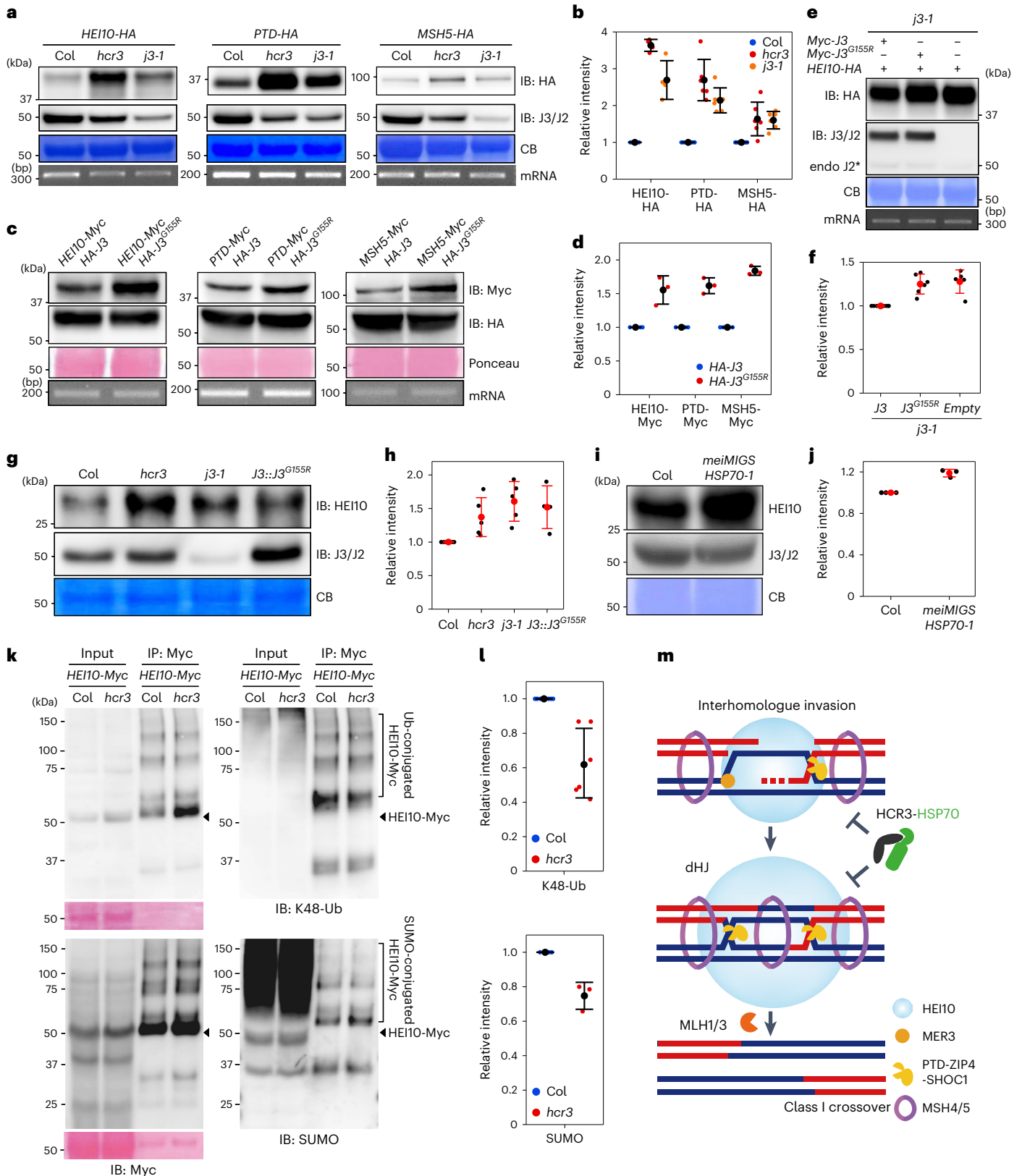
Besides the disaggregating and proteolytic roles of heat-induced chaperones comprising HSP40 and HSP70 in thermotolerance[32,35,45,46], our findings provide genetic and mechanistic insights into how the chaperone network of J3/J2-HSP70 limits meiotic crossovers and regulates interference by promoting degradation of pro-recombination factors.

Methods

Plant materials

The *A. thaliana* Columbia-0 (Col) accession was used as the wild type. Plants were grown in controlled growth rooms (20 °C, 50–60% humidity and 16 light/8 h dark photoperiod). Fluorescence-tagged lines for scoring seed and pollen tetrads were used as described[51,52]. The T-DNA insertion lines *j3-1* (SALK_132923)[36], *j3-3* (SAIL_1292_G03.V1), *j2-2* (SALK_071563)[37], *zip4-2* (SALK_068052)[16], *mus81-2* (SALK_107515)[6], *hsp101* (SALK_066374)[53] and *hei10-2* (SALK_012624)[16] were provided by the Arabidopsis Biological Resource Center. The *fancm-1* (ref. 7), *hcr1* and *hcr2* mutants were used as described[24,38]. The mutants of *recq4a recq4b* in Col and Ler accessions were used as described[54]. Genotyping of *hcr3* was performed by PCR using oligonucleotides *hcr3*-geno F and R (Supplementary Table 28), followed by BamHI (NEB) restriction endonuclease digestion.

Genetic screening and mapping of *hcr3*

Genetic screening and mapping of ethyl-methyl sulfonate (EMS)-derived *hcr3* using the *420* (*GR/++*) fluorescent seed reporter were performed as described[24]. Approximately 10,000 seeds of *420 GR/++* hemizygote seeds were treated with 0.3% (v/v) EMS and incubated for 12 h at room temperature (20 °C). Approximately 7,000 M_1 plants were grown and seeds of 12 M_1 plants were harvested and pooled for 600 M_2 pools. Approximately 150 seeds of each M_2 pool were preselected as *420/++* hemizygotes, grown, self-fertilized and used for *420* crossover frequency. To map the causal mutation of *hcr3*, the *hcr3* with the *420* reporter (*hcr3 GR/GR*) was crossed to Col plant. The backcrossed F_1 plants were self-fertilized to produce BC_1F_2 populations (Supplementary Fig. 1). BC_1F_2 seeds were preselected as measurable *420/++* BC_1F_2 hemizygous plants under an epifluorescence microscope and grown. F_3 seeds from individual BC_1F_2 plants were harvested and used to measure the *420* crossover frequency (cM) using CellProfiler, equipped with an automatic seed-scoring pipeline. Fifty BC_1F_2 plants with high crossover rates, like *hcr3*, were selected and ~5 mg of BC_1F_3 seeds from each BC_1F_2 individual were pooled and grown on 1/2 MS agar plates. Nuclear genomic DNA (gDNA) of pooled *hcr3* BC_1F_3 7-day seedlings was isolated and used for the preparation of a DNA sequencing library as described[24]. The SHOREmap (v.3.0) pipeline was used to map candidate mutations responsible for the *hcr3* phenotype, as described in refs. 24,55.

Plasmid construction for transgenic plants and transient assay

Plasmid construction in this study was performed using the Golden Gate cloning system as described[24] (Supplementary Table 28). For the complementation analysis of *j3*, the genomic regions of the *J3* promoter-5′-UTR, protein-coding region and 3′-UTR-terminator region were separately PCR-amplified and each PCR product was cloned to the universal Level 0 (Lv0) vector (pAGM9121). For N-terminal Myc or HA tagging, Lv0 vector of the J3 protein-coding region was assembled to Lv1 vector with Myc or HA vector, Lv0 vectors of the promoter-5′-UTR and 3′-UTR-terminator region. The Lv1 of *J3::Myc-J3* was assembled to an Lv2 binary vector (pAGM4723) with the antibiotic-resistant gene *BAR* containing an Lv1 vector (pICSL11017) and linker (pICH41744). The Lv2 vectors were electroporated into *Agrobacterium* strain GV3101-pSOUP and transformed into *Arabidopsis* by floral dipping.

To generate transgenic plants that express *J3* or *J3^G155R* under the *J3* or meiotic gene promoters, the genomic sequences of different gene promoters, *J3* and *J3^G155R* were cloned into the pAGM9121 vector using Golden Gate cloning. The Lv0 vectors for *J3* and meiotic gene promoters, *J3* or *J3^G155R*, were assembled into the Lv1 position 2 vector pICH47742 with the pICH41421. Each Lv1 vector was assembled into the pAGM4723 binary vector with pICSL11017 and pICH41744.

For *meiMIGS-HSP70* and *meiMIGS-J2* plants, complementary DNA regions of *HSP70-1*, *HSP70-3* and *J2* were cloned into the Lv0 vector (pAGM9121) following amplification using forward primers that included the miR173 target sequence and reverse primers (Supplementary Table 28). The *DMC1* promoter and *MIGS-HSP70* Lv0 vectors or the *SPO11-1* promoter and *MIGS-J2* Lv0 vectors were assembled into the Lv1 position 2 vector (pICH47742) with the *NOPALINE SYNTHASE GENE* (*NOS*) terminator (pICH41421). The Lv1 vector was assembled to the pAGM4723 binary vector with pICSL11017 and pICH41744.

To generate *j3* knockout alleles using CRISPR/Cas9 mutagenesis, Gateway *pEn-C1.1* (Addgene plasmid no. 61479) and *pDe-CAS9* (Addgene plasmid no. 61433) plasmids were used and two sgRNAs were cloned using complementary sgRNA oligonucleotides (Supplementary Table 28), as previously described[56].

For the *Arabidopsis* transient assay, the full-length protein-coding region lacking stop codons of meiotic genes was cloned to pAGM9121 universal vector. The Lv0 vectors were assembled in the Lv1 vector (pICH4772), with the *35S* promoter (pICH51266), C-terminal epitope-tagged vector (pICSLl50010 or pICSL50009) and *NOS* terminator (pICH41421). For TurboID-based proximity labelling assays of TurboID-J3 (ref. 57), TurboID clone was assembled to the N-terminal of *J3* in the Lv1 vector with Lv0 vectors of the *35S* promoters or *J3* promoters, *J3* coding region and *NOS* terminator.

High-throughput measurement crossover frequency and interference ratio

In the seed FTL system, crossover frequency was measured using a CellProfiler image-analysis pipeline that allows for the analysis of fluorescent and non-fluorescent seeds from *FTL/++* hemizygote plants. CellProfiler detects and analyses the numbers of green-only fluorescent seeds (N_{Green}), red-only fluorescent seeds (N_{Red}) and total seeds (N_{Total})[58]. Crossover frequency (cM) is calculated using the formula: cM = 100 $\times (1 - [1 - 2(N_{Green} + N_{Red})/N_{Total}]^{1/2})$ (refs. 52,59). In the pollen tetrad FTL system, DeepTetrad, a deep learning-based image-analysis pipeline was used for the measurement of IFR in two- or three-colour FTLs, as described in refs. 40,60. Using three-colour FTLs that have two intervals, IFR was calculated as the ratio of the map distance with adjacent crossover to the map distance without adjacent crossover. Two-sided Welch's *t*-test was used to test whether crossover frequency and IFR varied significantly among genotypes.

Genotyping-by-sequencing for mapping genomic crossover sites

For sex-average crossover maps, Col and *J3::J3^G155R* Col in *420* background were crossed with Ler to produce Col × Ler and *J3::J3^G155R*/+ Col × Ler F_1 hybrid plants, respectively. F_1 plants were self-fertilized for the production of F_2 individuals. For sex-specific crossover maps, the Col × Ler and *J3^G155R*/+ Col × Ler F_1 hybrid plants were reciprocally crossed with Ler. The backcrossed F_1 individuals were used for GBS. For crossover maps in the *recq4a recq4b* background, the *J3^G155R* Col plant was crossed with *recq4a recq4b* Col and then the F_1 plant (*J3^G155R*/+ *recq4a*/+ *recq4b*/+) was crossed with the *recq4a recq4b* Ler plant to produce *J3^G155R*/+ *recq4a recq4b* Col × Ler F_1 hybrid. Individual plants were grown on soil for 3 weeks. The gDNA was extracted from two to three adult leaves per individual plant using the CTAB method for the preparation of sequencing libraries as described in refs. 11,24. Briefly, 150 ng of gDNA from each F_2 plant was quantified using Qubit dsDNA Broad Range assay kit (Thermo Fisher) and fragmented using dsDNA Shearase (Zymo Research) and used to generate one sequencing library per plant. The 96 barcoded libraries were pooled and subjected to paired-end 150 base pair sequencing using an Illumina HiSeqX

instrument (Macrogen). The TIGER pipeline was applied to analyse the sequencing data and map precisely crossovers as described in ref. 39.

RNA sequencing

RNA extraction and sequencing library construction were performed as described[61]. Total RNA was extracted from the seedlings and unopened floral buds that were smaller than ~0.6 mm using RNeasy Plant mini kit (QIAGEN). A Ribo-Zero magnetic kit (MRZPL116, Epicentre) was used for ribosomal RNA depletion. In addition, 50 ng of rRNA-depleted RNA was used to construct sequencing libraries using a ScriptSeq v.2 RNA-seq Library Preparation Kit (SSV21124, Epicentre). Twelve PCR cycles were used for amplification of the libraries using ScriptSeq Index PCR Primers (RSBC10948, Epicentre). Three replicates of the RNA-seq libraries were generated for each genotype with different indexes. Sequencing was conducted on an Illumina HiSeq instrument (BGI). Adaptor sequences were trimmed from the raw reads with Trim Galore (v.0.6.6) with parameters -q 0 --stringency 3 --length 20. Trimmed reads were aligned to the TAIR10 reference using STAR (v.2.7.3) with default parameters. The number of reads mapped to exons was calculated using featureCounts (v.2.0.1) with default parameters[62]. Differentially expressed genes and sequencing reads were analysed among meiosis-related genes (inhouse list) with the R package DESeq2 using a Benjamini−Hochberg adjusted $P < 0.01$ as cutoff[63].

RT−qPCR analysis

Male meiocytes were isolated from stage 9 floral buds by squeezing them between a glass slide and coverslip, as previously described[64]. Total RNA from purified male meiocytes or floral buds <0.6 mm was isolated using TRIzol reagent (Invitrogen) and used for RT−qPCR using a reverse transcription kit (Enzynomics, EZ405S). Quantitative PCR was performed using a CFX real-time PCR detection system (Bio-Rad). *TUB2* (*TUBULIN BETA CHAIN2*) was used as a reference for normalization. RT−qPCR was conducted with at least three biological replicates and two or three technical repeats per replicate.

Purification of J3 protein and antibody generation

The full-length *J3* coding sequence (At3g44110) was amplified from *Arabidopsis* cDNA using pQE-J3_F and pQE-J3_R primers. The PCR product was then cloned into the pQE-80L expression vector using the BamHI and HindIII restriction sites via the Gibson assembly cloning system to generate an N-terminal 6×-His tagged recombinant protein. The resulting construct was transformed into *Escherichia coli* strain BL21 (DE3) RIL and the recombinant J3 protein was purified as previously described[38]. A polyclonal antibody against the purified recombinant J3 protein was raised in mice (Abclon).

Immunocytological analysis

Chromosome spreads of pollen mother cells from fixed buds and staining with DAPI were performed as described in ref. 65. Immunostaining of MLH1 was performed on acetic acid chromosome spreads using fixed buds as described in ref. 65. Immunostainings of ASY1, RAD51, ZYP1, J3 and HEI10 were performed using fresh floral buds as described[22] and as in ref. 18 for late-pachytene nuclei. The following antibodies were used: α-ASY1 (rat, 1:500 dilution; guinea-pig, 1:500 dilution)[22], α-ZYP1 (rabbit, 1:200 dilution; rat, 1:500 dilution)[66], RAD51 (rabbit, 1:300 dilution)[22], α-MLH1 (rabbit, 1:200 dilution)[65], α-J3 (mouse, 1:500 dilution) and α-HEI10 (chicken, 1:1,000; rabbit, 1:500 dilution)[16]. For ASY1, RAD51 and MLH1, microscopy was performed using a DeltaVision personal DV microscope (Applied precision/GE Healthcare) equipped with a CCD Coolsnap HQ2 camera (Photometrics). Images were captured and analysed using SoftWoRx software v.5.5 (Applied precision/GE Healthcare). For ASY1 and RAD51 co-immunostaining of leptotene-stage nuclei, individual cell images were acquired as Z-stacks of ten optical sections of 0.2 μm each and

the maximum intensity projection for each cell was determined using ImageJ. Numbers of MLH1 foci per cell and RAD51 foci per cell associated with ASY1 were counted manually. Wilcoxon tests were used to assess significant differences between genotypes for MLH1 and RAD51 foci counts.

Immunolocalization of MLH1 was performed on three-dimensional preserved meiocytes as previously described[67] with the following modifications: 5−10 flower buds were used for a single gel pad and were digested for 20 min at 37 °C after fixation in a digestion mix of 0.3% (w/v) pectolyase Y-23 (MP Biomedicals), 0.3% (w/v) Drise-lase (Sigma) and 0.3% (w/v) Cellulase Onozuka R10 (Duchefa). The gel pads were mounted in Vectashield (Vectorlabs) and primary antibodies were incubated for 48−72 h. After treatment with primary and secondary antibodies, gels were washed four times in PBS with 0.1% Triton for 30 min. Secondary antibodies were diluted 1:250. Primary antibodies were rabbit α-MLH1 (1:500)[65], chicken α-HEI10 (1:10,000)[16] and rat α-ZYP1 (1:250)[66]. Secondary antibodies were conjugated with Alexa 488, Alexa 568 or Alexa 647 (Thermo Fisher Scientific). Observations were made using either a Zeiss AxioImager 2 microscope or a Leica confocal microscope TCS SP8 AOBS (Acousto-Optical Beam Splitter). On the Zeiss AxioImager 2 microscope, observations were made using a ×60/1.42 oil objective lens with 1.59 auxiliary magnification and images were captured with a Zeiss AxioCam MR camera driven by Axiovision 4.7 at 0.24 μm intervals along the z axis. On the Leica SP8 system, the images were acquired as described[68] but using an HC PL APO CS2 ×63/1.4 NA immersion objective lens. Fluorescent signals were recorded using LASX software in the Lightning mode. Z-stacks at 0.13 μm intervals were acquired and deconvolved using Lightning default parameters and the adaptative-vectashield option. All images were further processed using Imaris software (https://www.oxinst.com/).

For HEI10 and ZYP1 immunostaining in late-pachytene nuclei, three-dimensional-structured illumination microscopy (3D-SIM) was performed using a Zeiss Elyra PS1 microscope as described in ref. 18. Individual bivalents were traced using the SNT Fiji plugin. Trace fluorescence intensity quantification and HEI10 peak identification were performed using the bespoke image-analysis pipeline described in ref. 18. Late-pachytene data were collected from 120 bivalents from 24 nuclei from four *hcr3* plants and 135 bivalents from 27 nuclei from four Col plants. The peak detection algorithm encountered problems for three *hcr3* bivalents and one Col bivalent, which were excluded from downstream data analysis.

Mathematical modelling

Simulations of the 'coarsening model' for crossover patterning were performed as described in ref. 18. For Col simulations, parameter values were identical to those used in wild-type simulations from ref. 18. For *hcr3* simulations, all parameter values were fixed, except for those parameters specifying the initial concentrations of HEI10, both on the SC and at recombination intermediates, which were each increased to be 1.3× wild-type levels.

Yeast two-hybrid (Y2H) assay

Y2H assay was performed as described in ref. 24. The open reading frames of *J3*, except J domain and meiotic genes, were cloned into pGBKT7 BD and pGADT7 AD vectors (Clontech, 630490) using BamHI and StuI sites, using a Gibson assembly cloning system (NEB E2621L). Plasmids of cloned BD and AD vectors were cotransformed into yeast strain AH109 and selected on synthetic dropout medium lacking leucine (−L) and tryptophan (−T). The colonies of yeast transformant cells were streaked onto both (−LT) and (−LTH (histidine) A (adenine)) synthetic media and grown for 3−5 d at 30 °C. The cells grown in synthetic medium (−LT) were grown until optical density $OD_{600} = 1$ and diluted 10-, 100- and 1,000-fold in water and spotted on synthetic medium (−LTHA) for 3−7 d.

Co-immunoprecipitation analysis and proximity label assay using *Arabidopsis* protoplast transient expression

Arabidopsis protoplasts and plasmid DNA were prepared and co-immunoprecipitation analysis was performed as described in ref. 24. Furthermore, 40 μg of Myc- and HA-tagged DNA plasmids were co-transfected into ~20×10^3 protoplasts or separately transfected as a negative control and incubated for 6–12 h at room temperature (20 °C). Protoplasts were centrifuged and harvested and total protein was extracted using extraction buffer (50 mM Tris-HCl pH 7.5, 100 mM NaCl, 5 mM EDTA, 1 mM dithiothreitol, protease inhibitor cocktail (Roche) and 1% Triton X-100). The isolated proteins were separated by SDS–polyacrylamide gel electrophoresis (SDS–PAGE) using 8% polyacrylamide gels, transferred to a nitrocellulose membrane and detected with α-HA (Roche 12013819001, 1:2,000 dilution) or α-Myc (Santa Cruz, sc-40, 1:2,000 dilution) antibodies. For co-immunoprecipitation analysis, transfected protoplasts were lysed with IP buffer (50 mM Tris-HCl pH 7.5, 100 mM NaCl, 1 mM EDTA, 0.5% Triton X-100, 10% glycerol and protease inhibitor cocktail). Lysates were incubated with 1 μg of α-HA for 12 h with rotation at 4 °C. The protoplast lysate and antibody mixture were incubated with Dynabeads Protein G (Invitrogen, 10004D) for a further 2 h. Protein-coated Dynabeads were washed with IP buffer three times. Proteins were extracted using an extraction buffer and analysed by immunoblotting using α-Myc antibodies.

For TurboID-based proximity label assay, transfected protoplasts were incubated with biotin (5 μM) for 1 h and lysed with IP buffer. Lysates were incubated with Dynabeads MyOne Streptavidin C1 (Invitrogen, 65001) in the equilibration buffer (50 mM Tris pH 7.5, 150 mM NaCl, 0.05% Triton X-100, 1 mM dithiothreitol) overnight at 4 °C on a rotor wheel. The beads were washed with wash buffer 1 (50 mM Hepes pH 7.5, 500 mM NaCl, 1 mM EDTA, 1% Triton X-100, 0.5% Na-deoxycholate), wash buffer 2 (10 mM Tris pH 8, 250 mM LiCl, 1 mM EDTA, 0.5% NP-40, 0.5% Na-deoxycholate) and wash buffer 3 (50 mM Tris pH 7.5, 50 mM NaCl, 0.1% NP-40). Proteins were eluted by boiling the beads for 15 min at 98 °C in elution buffer (10 mM Tris pH 7.5, 2% SDS, 5% beta mercaptoethanol, 2 mM biotin) and used for immunoblotting.

Immunoblot analysis of meiotic proteins in *Arabidopsis*

Approximately 0.1 g of floral buds smaller than ~0.6 mm were sampled and liquid nitrogen was used to grind the unopened buds with a mortar and pestle. Total protein was extracted using an extraction buffer (50 mM Tris-HCl pH 7.5, 100 mM NaCl, 5 mM EDTA, 1 mM dithiothreitol, protease inhibitor cocktail (Roche) and 1% Triton X-100). Extracted proteins were separated by SDS–PAGE using 8–12% polyacrylamide gels and transferred to PVDF membranes (Immobilon-P, Merck Millipore). The epitope-tagged proteins were detected using α-HA (Roche 12013819001, 1:2,000 dilution) or α-Myc (Santa Cruz sc-40, 1:2,000 dilution) antibodies. For HEI10 immunoblot analysis, Western BLoT Blocking Buffer (T7131A, Takara) was added to the transferred membrane and incubated on the shaker at 20 °C for 60 min. The membranes were washed using 1× PBS-T and then incubated with chicken anti-HEI10 (1:1,000 dilution, IJPB) at 4 °C overnight. After washing three times, the membranes were incubated with horseradish peroxidase (HRP)-conjugated goat anti-chicken IgY (1:2,000 dilution, Abcam Ab97135) for 1 h at 20 °C. The signals were detected using chemiluminescence with secondary horseradish peroxidase-conjugated antibodies (Clarity Western ECL, Bio-Rad). Coomassie blue or Ponceau S staining of the membrane was used and shown for a loading control.

To detect ubiquitin- or SUMO-conjugated HEI10-Myc proteins, total protein was extracted from flower buds smaller than 0.6 mm of 6-week-old *HEI10::HEI10-Myc* and *hcr3 HEI10::HEI10-Myc* using lysis buffer (25 mM HEPES, 5 mM EDTA, 2% SDS and 1× protease inhibitor cocktail). Protein concentration was determined by bicinchoninic acid assay (Thermo Scientific, 23225). For immunoprecipitation of HEI10-Myc, 5 mg of protein lysates were incubated with 4 μg of α-Myc (Santa Cruz, sc-9E10) in IP buffer (50 mM Tris-HCl pH 7.5, 100 mM NaCl,

1 mM EDTA, 0.5% Triton X-100, 10% glycerol and protease inhibitor cocktail) for 12 h at 4 °C. The lysate and antibody mixture were incubated with Dynabeads Protein G (Invitrogen, 10004D) for 2 h at 4 °C and Dynabeads were washed with IP buffer three times. α-K48-linkage specific polyubiquitin (Cell Signaling 12805, 1:1,000 dilution), α-SUMO1 (Abcam ab5316, 1:5,000 dilution) and α-Myc (Santa Cruz, sc-40 HRP, 1:1,000 dilution) antibodies were used to detect modified HEI10-Myc proteins for immunoblot analysis. For reprobing immunoblot, the membrane was incubated in stripping buffer (62.5 Tris-HCl pH 6.8, 0.5% SDS, 0.8% beta mercaptoethanol) for 40 min at 50 °C.

Statistics and reproducibility
All experiments with representative images were conducted at least three times with similar results.

Reporting summary
Further information on research design is available in the Nature Portfolio Reporting Summary linked to this article.

Data availability
Seeds of *Arabidopsis* transgenic plants used for this study are freely available on request. GBS data in this study are available in the ArrayExpress database at EMBL-EBL (http://www.ebi.ac.uk/arrayexpress) under the accession numbers E-MTAB-10168, E-MTAB-11586, E-MTAB-12663, E-MTAB-12692, E-MTAB-12694, E-MTAB-12695, E-MTAB-12696, E-MTAB-12697, E-MTAB-12726 and E-MTAB-13412–13415. RNA-seq data have been deposited at EMBL-EBI under accession numbers E-MTAB-12699 and E-MTAB-13417. Source data are provided with this paper.

Code availability
All custom codes involved in the paper are available at https://github.com/KyuhaChoi-Lab/HCR3.

References
1. Villeneuve, A. M. & Hillers, K. J. Whence meiosis? *Cell* **106**, 647–650 (2001).
2. Hunter, N. Meiotic recombination: the essence of heredity. *Cold Spring Harb. Perspect. Biol.* **7**, 1–36 (2015).
3. Mercier, R., Mézard, C., Jenczewski, E., Macaisne, N. & Grelon, M. The molecular biology of meiosis in plants. *Annu. Rev. Plant Biol.* **66**, 297–327 (2015).
4. Pyatnitskaya, A., Borde, V. & De Muyt, A. Crossing and zipping: molecular duties of the ZMM proteins in meiosis. *Chromosoma* **128**, 181–198 (2019).
5. Berchowitz, L. E. & Copenhaver, G. P. Genetic interference: don't stand so close to me. *Curr. Genomics* **11**, 91–102 (2010).
6. Berchowitz, L. E., Francis, K. E., Bey, A. L. & Copenhaver, G. P. The role of AtMUS81 in interference-insensitive crossovers in *A. thaliana*. *PLoS Genet.* **3**, e132 (2007).
7. Crismani, W. et al. FANCM limits meiotic crossovers. *Science* **336**, 1588–1590 (2012).
8. Séguéla-Arnaud, M. et al. Multiple mechanisms limit meiotic crossovers: TOP3α and two BLM homologs antagonize crossovers in parallel to FANCM. *Proc. Natl Acad. Sci. USA* **112**, 4713–4718 (2015).
9. Agarwal, S. & Roeder, G. S. Zip3 provides a link between recombination enzymes and synaptonemal complex proteins. *Cell* **102**, 245–255 (2000).
10. De Muyt, A. et al. E3 ligase Hei10: a multifaceted structure-based signaling molecule with roles within and beyond meiosis. *Genes Dev.* **28**, 1111–1123 (2014).
11. Ziolkowski, P. A. et al. Natural variation and dosage of the HEI10 meiotic E3 ligase control *Arabidopsis* crossover recombination. *Genes Dev.* **31**, 306–317 (2017).

12. Qiao, H. et al. Antagonistic roles of ubiquitin ligase HEI10 and SUMO ligase RNF212 regulate meiotic recombination. *Nat. Genet.* **46**, 194–199 (2014).

13. Reynolds, A. et al. RNF212 is a dosage-sensitive regulator of crossing-over during mammalian meiosis. *Nat. Genet.* **45**, 269–278 (2013).

14. Bhalla, N., Wynne, D. J., Jantsch, V. & Dernburg, A. F. ZHP-3 acts at crossovers to couple meiotic recombination with synaptonemal complex disassembly and bivalent formation in *C. elegans*. *PLoS Genet.* **4**, e1000235 (2008).

15. Serra, H. et al. Massive crossover elevation via combination of HEI10 and recq4a recq4b during *Arabidopsis* meiosis. *Proc. Natl Acad. Sci. USA* **115**, 2437–2442 (2018).

16. Chelysheva, L. et al. The *Arabidopsis* HEI10 is a new ZMM protein related to Zip3. *PLoS Genet.* **8**, e1002799 (2012).

17. Kong, A. et al. Sequence variants in the RNF212 gene associate with genome-wide recombination rate. *Science* **319**, 1398–1401 (2008).

18. Morgan, C. et al. Diffusion-mediated HEI10 coarsening can explain meiotic crossover positioning in *Arabidopsis*. *Nat. Commun.* **12**, 4674 (2021).

19. Banani, S. F., Lee, H. O., Hyman, A. A. & Rosen, M. K. Biomolecular condensates: organizers of cellular biochemistry. *Nat. Rev. Mol. Cell Biol.* **18**, 285–298 (2017).

20. France, M. G. et al. ZYP1 is required for obligate cross-over formation and cross-over interference in *Arabidopsis*. *Proc. Natl Acad. Sci. USA* **118**, e2021671118 (2021).

21. Capilla-Pérez, L. et al. The synaptonemal complex imposes crossover interference and heterochiasmy in *Arabidopsis*. *Proc. Natl Acad. Sci. USA* **118**, e2023613118 (2021).

22. Lambing, C., Kuo, P. C., Tock, A. J., Topp, S. D. & Henderson, I. R. ASY1 acts as a dosage-dependent antagonist of telomere-led recombination and mediates crossover interference in *Arabidopsis*. *Proc. Natl Acad. Sci. USA* **24**, 13647–13658 (2020).

23. Zhang, L. et al. Topoisomerase II mediates meiotic crossover interference. *Nature* **511**, 551–556 (2014).

24. Nageswaran, D. C. et al. HIGH CROSSOVER RATE1 encodes PROTEIN PHOSPHATASE X1 and restricts meiotic crossovers in *Arabidopsis*. *Nat. Plants* **7**, 452–467 (2021).

25. Ahuja, J. S. et al. Control of meiotic pairing and recombination by chromosomally tethered 26S proteasome. *Science* **355**, 408–411 (2017).

26. Haversat, J. et al. Robust designation of meiotic crossover sites by CDK-2 through phosphorylation of the MutSγ complex. *Proc. Natl Acad. Sci. USA* **119**, e2117865119 (2022).

27. He, W. et al. Regulated proteolysis of MutSγ controls meiotic crossing over. *Mol. Cell* **78**, 168–183 (2020).

28. Cheng, C.-H. et al. SUMO modifications control assembly of synaptonemal complex and polycomplex in meiosis of *Saccharomyces cerevisiae*. *Genes Dev.* **20**, 2067–2081 (2006).

29. Bhagwat, N. R. et al. SUMO is a pervasive regulator of meiosis. *eLife* **10**, e57720 (2021).

30. He, W. et al. SUMO fosters assembly and functionality of the MutSγ complex to facilitate meiotic crossing over. *Dev. Cell* **56**, 2073–2088 (2021).

31. Rao, H. B. D. P. et al. A SUMO-ubiquitin relay recruits proteasomes to chromosome axes to regulate meiotic recombination. *Science* **355**, 402–407 (2017).

32. Rosenzweig, R., Nillegoda, N. B., Mayer, M. P. & Bukau, B. The Hsp70 chaperone network. *Nat. Rev. Mol. Cell Biol.* **20**, 665–680 (2019).

33. Jiang, Y., Rossi, P. & Kalodimos, C. G. Structural basis for client recognition and activity of Hsp40 chaperones. *Science* **365**, 1313–1319 (2019).

34. Lee, D. H., Sherman, M. Y. & Goldberg, A. L. Involvement of the molecular chaperone Ydj1 in the ubiquitin-dependent degradation of short-lived and abnormal proteins in *Saccharomyces cerevisiae*. *Mol. Cell. Biol.* **16**, 4773–4781 (1996).

35. Mogk, A., Bukau, B. & Kampinga, H. H. Cellular handling of protein aggregates by disaggregation machines. *Mol. Cell* **69**, 214–226 (2018).

36. Shen, L., Kang, Y. G. G., Liu, L. & Yu, H. The J-domain protein J3 mediates the integration of flowering signals in *Arabidopsis*. *Plant Cell* **23**, 499–514 (2011).

37. Barghetti, A. et al. Heat-shock protein 40 is the key farnesylation target in meristem size control, abscisic acid signaling and drought resistance. *Genes Dev.* **31**, 2282–2295 (2017).

38. Kim, J. et al. *Arabidopsis* HEAT SHOCK FACTOR BINDING PROTEIN is required to limit meiotic crossovers and HEI10 transcription. *EMBO J.* **41**, e109958 (2022).

39. Rowan, B. A., Patel, V., Weigel, D. & Schneeberger, K. Rapid and inexpensive whole-genome genotyping-by-sequencing for crossover localization and fine-scale genetic mapping. *G3* **5**, 385–398 (2015).

40. Berchowitz, L. E. & Copenhaver, G. P. Fluorescent *Arabidopsis* tetrads: a visual assay for quickly developing large crossover and crossover interference data sets. *Nat. Protoc.* **3**, 41–50 (2008).

41. Modliszewski, J. L. et al. Elevated temperature increases meiotic crossover frequency via the interfering (Type I) pathway in *Arabidopsis thaliana*. *PLoS Genet.* **14**, e1007384 (2018).

42. Lloyd, A., Morgan, C., Franklin, F. C. H. & Bomblies, K. Plasticity of meiotic recombination rates in response to temperature in *Arabidopsis*. *Genetics* **208**, 1409–1420 (2018).

43. Fang, N. N. et al. Rsp5/Nedd4 is the main ubiquitin ligase that targets cytosolic misfolded proteins following heat stress. *Nat. Cell Biol.* **16**, 1227–1237 (2014).

44. de Felippes, F. F., Wang, J. & Weigel, D. MIGS: miRNA-induced gene silencing. *Plant J.* **70**, 541–547 (2012).

45. McLoughlin, F., Kim, M., Marshall, R. S., Vierstra, R. D. & Vierling, E. HSP101 interacts with the proteasome and promotes the clearance of ubiquitylated protein aggregates. *Plant Physiol.* **180**, 1829–1847 (2019).

46. Yoo, H., Bard, J. A. M., Pilipenko, E. V. & Drummond, D. A. Chaperones directly and efficiently disperse stress-triggered biomolecular condensates. *Mol. Cell* **82**, 741–755 (2022).

47. Prusicki, M. A. et al. Live cell imaging of meiosis in *Arabidopsis thaliana*. *eLife* **8**, e42834 (2019).

48. Fozard, J. A., Morgan, C. & Howard, M. Coarsening dynamics can explain meiotic crossover patterning in both the presence and absence of the synaptonemal complex. *eLife* **12**, e79408 (2023).

49. Durand, S. et al. Joint control of meiotic crossover patterning by the synaptonemal complex and HEI10 dosage. *Nat. Commun.* **13**, 5999 (2022).

50. Morgan, C. et al. Evolution of crossover interference enables stable autopolyploidy by ensuring pairwise partner connections in *Arabidopsis arenosa*. *Curr. Biol.* **31**, 4713–4726 (2021).

51. Wu, G., Rossidivito, G., Hu, T., Berlyand, Y. & Poethig, R. S. Traffic lines: new tools for genetic analysis in *Arabidopsis thaliana*. *Genetics* **200**, 35–45 (2015).

52. Melamed-Bessudo, C., Yehuda, E., Stuitje, A. R. & Levy, A. A. A new seed-based assay for meiotic recombination in *Arabidopsis thaliana*. *Plant J.* **43**, 458–466 (2005).

53. Charng, Y.-Y., Liu, H.-C., Liu, N.-Y., Hsu, F.-C. & Ko, S.-S. *Arabidopsis* Hsa32, a novel heat shock protein, is essential for acquired thermotolerance during long recovery after acclimation. *Plant Physiol* **140**, 1297–1305 (2006).

54. Fernandes, J. B., Seguela-Arnaud, M., Larcheveque, C., Lloyd, A. H. & Mercier, R. Unleashing meiotic crossovers in hybrid plants. *Proc. Natl Acad. Sci. USA* **115**, 2431–2436 (2017).

55. Schneeberger, K. et al. SHOREmap: simultaneous mapping and mutation identification by deep sequencing. *Nat. Methods* **6**, 550–551 (2009).

56. Schiml, S., Fauser, F. & Puchta, H. The CRISPR/Cas system can be used as nuclease for in planta gene targeting and as paired nickases for directed mutagenesis in *Arabidopsis* resulting in heritable progeny. *Plant J.* **80**, 1139–1150 (2014).

57. Mair, A., Xu, S.-L., Branon, T. C., Ting, A. Y. & Bergmann, D. C. Proximity labeling of protein complexes and cell type specific organellar proteomes in *Arabidopsis* enabled by TurboID. *eLife* **8**, e47864 (2019).

58. van Tol, N., Rolloos, M., van Loon, P. & van der Zaal, B. J. MeioSeed: a CellProfiler-based program to count fluorescent seeds for crossover frequency analysis in *Arabidopsis thaliana*. *Plant Methods* **14**, 32 (2018).

59. Ziolkowski, P. A. et al. Juxtaposition of heterozygous and homozygous regions causes reciprocal crossover remodelling via interference during *Arabidopsis* meiosis. *eLife* **4**, e03708 (2015).

60. Lim, E.-C. et al. DeepTetrad: high-throughput image analysis of meiotic tetrads by deep learning in *Arabidopsis thaliana*. *Plant J.* **101**, 473–483 (2020).

61. Choi, K. et al. Nucleosomes and DNA methylation shape meiotic DSB frequency in *Arabidopsis thaliana* transposons and gene regulatory regions. *Genome Res.* **28**, 532–546 (2018).

62. Liao, Y., Smyth, G. K. & Shi, W. FeatureCounts: an efficient general purpose program for assigning sequence reads to genomic features. *Bioinformatics* **30**, 923–930 (2014).

63. Love, M. I., Huber, W. & Anders, S. Moderated estimation of fold change and dispersion for RNA-seq data with DESeq2. *Genome Biol.* **15**, 550 (2014).

64. Walker, J. et al. Sexual-lineage-specific DNA methylation regulates meiosis in *Arabidopsis*. *Nat. Genet.* **50**, 130–137 (2018).

65. Chelysheva, L. et al. An easy protocol for studying chromatin and recombination protein dynamics during *Arabidopsis thaliana* meiosis: immunodetection of cohesins, histones and MLH1. *Cytogenet. Genome Res.* **129**, 143–153 (2010).

66. Higgins, J. D., Sanchez-Moran, E., Armstrong, S. J., Jones, G. H. & Franklin, F. C. H. The *Arabidopsis* synaptonemal complex protein ZYP1 is required for chromosome synapsis and normal fidelity of crossing over. *Genes Dev.* **19**, 2488–2500 (2005).

67. Hurel, A. et al. A cytological approach to studying meiotic recombination and chromosome dynamics in *Arabidopsis thaliana* male meiocytes in three dimensions. *Plant J.* **95**, 385–396 (2018).

68. Vrielynck, N. et al. Conservation and divergence of meiotic DNA double strand break forming mechanisms in *Arabidopsis thaliana*. *Nucleic Acids Res.* **49**, 9821–9835 (2021).

Author contributions

H.K., J.K., C.M., I.R.H. and K.C. designed the study. H.K., J.K., N.S., P.K., C.M., A.C., D.B., J.P., Y.L., Y.M.P., J.G., A.H., C.L. and K.C. performed experiments. H.K., J.K., D.B, J.P., Y.L., Y.M.P., I.H., R.M., I.R.H. and K.C. contributed to genetics, genomics and biochemical results. H.K., P.K., C.M., A.C., J.G., A.H., C.L. and M.G. contributed to cytological data. C.M. generated the data of HEI10 foci. P.K., A.C., J.G., A.H., C.L. and M.G. contributed to quantification of MLH1 foci. H.K., J.K., N.S., P.K., C.M., A.C., D.B., J.P., Y.L., Y.M.P., J.A.F, C.L., M.H., M.G., I.R.H. and K.C. analysed the results. N.S. conducted analyses of GBS and RNA-seq data. J.A.F analysed the HEI10 coarsening model. C.L., M.H., M.G., I.H., I.R.H. and K.C. contributed to the supervision. H.K., J.K. and K.C. wrote and revised the paper. All authors commented, discussed and provided input on the paper.

Competing interests

The authors declare no competing interests.

Additional information

Extended data is available for this paper at https://doi.org/10.1038/s41477-024-01633-y.

Supplementary information The online version contains supplementary material available at https://doi.org/10.1038/s41477-024-01633-y.

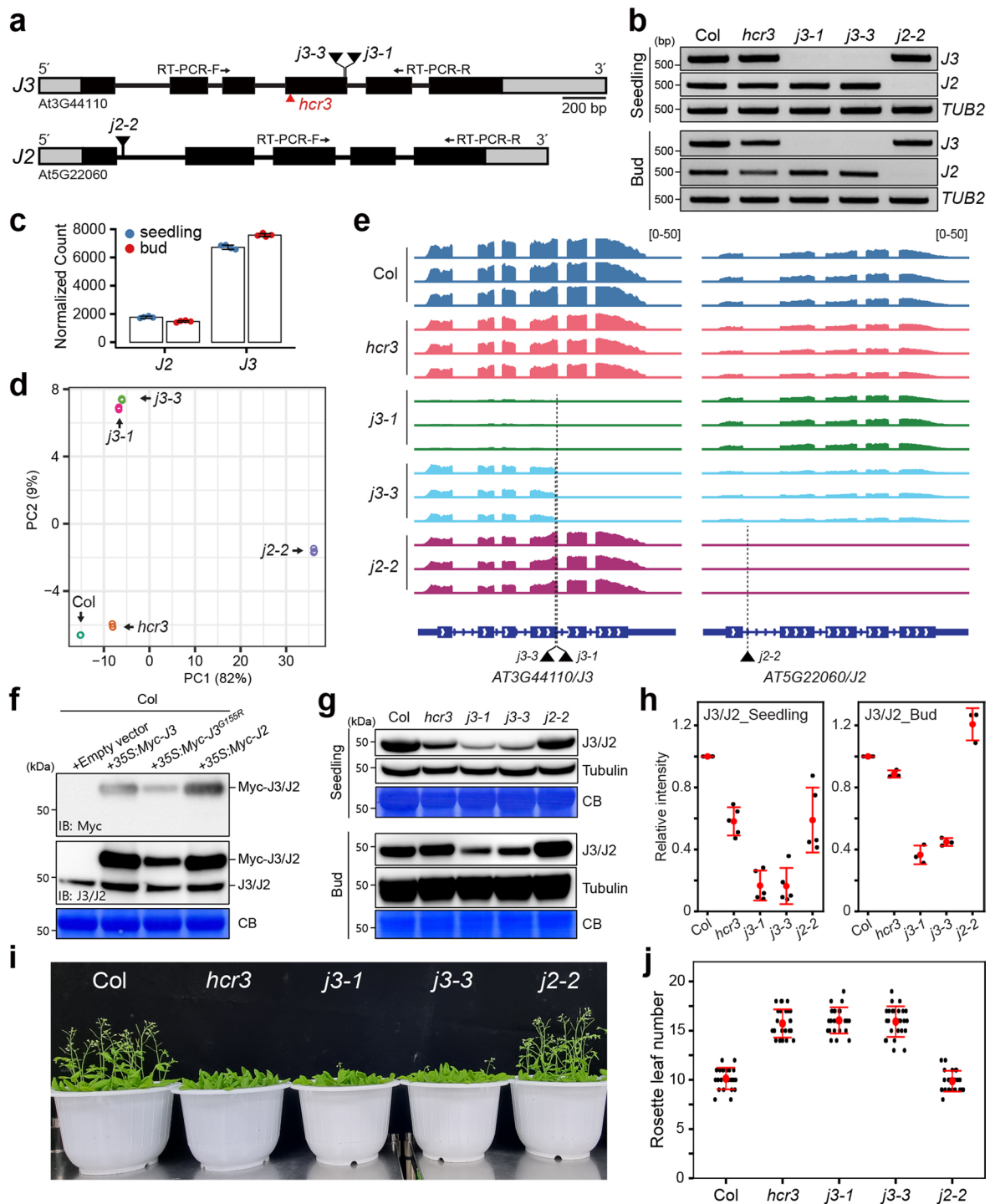**Correspondence and requests for materials** should be addressed to Kyuha Choi.

Peer review information *Nature Plants* thanks Zhukuan Cheng and the other, anonymous, reviewer(s) for their contribution to the peer review of this work.

Reprints and permissions information is available at www.nature.com/reprints.

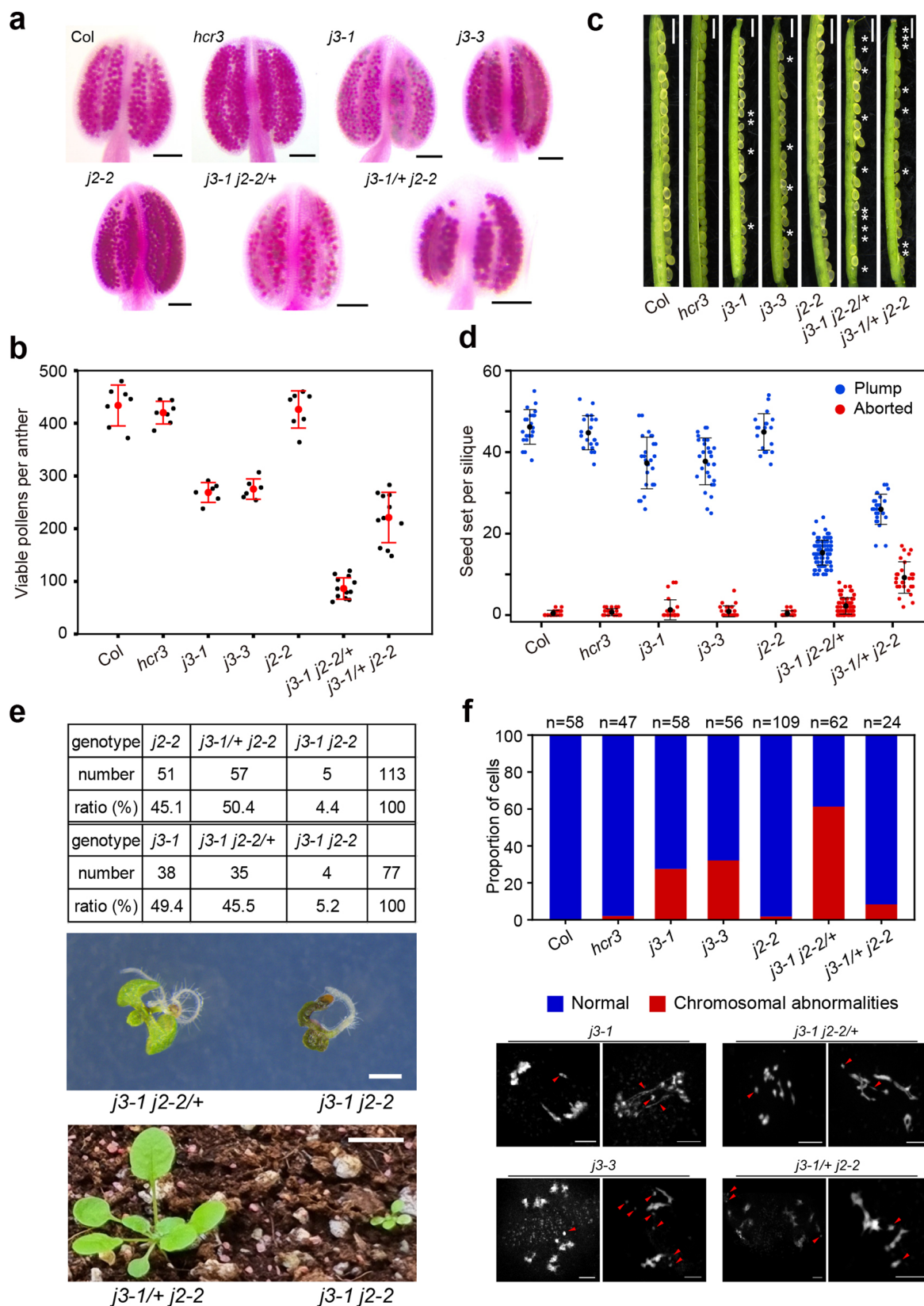**Extended Data Fig. 1 | Characterization of *j3* and *j2* T-DNA insertion mutants.** **a**, Gene structures for *J3* and *J2*. Positions of T-DNA insertion (black triangles), *hcr3* mutation (red triangle) and RT–PCR primers (arrows) are shown. **b**, Agarose gels showing RT–PCR products of *J3* and *J2* in Col, *hcr3*, *j3-1*, *j3-3* and *j2-2*. **c**, Plot showing normalized transcript reads for *J3* and *J2* in RNA-seq of Col seedlings (*J3*, $n = 4$, *J2*, $n = 4$) and buds (*J3*, $n = 4$, *J2*, $n = 4$). Data are presented as mean values ± s.d. values of normalized transcript reads. $n =$ the number of biologically independent samples. **d**, Principle component analysis of three replicates of RNA-seq libraries in Col, *hcr3*, *j3-1*, *j3-3* and *j2-2* seedlings. **e**, As for (**d**) but showing integrative genomic viewer windows showing the transcript levels for *J3* and *J2*. **f**, Immunoblot analysis of transiently expressed epitope Myc-tagged and endogenous J3 and J2 in Col protoplasts. IB, immunoblot. CB, Coomassie blue. Anti-J3 antibody detects both J3 and J2 proteins (J3/J2). **g,h**, Immunoblot (**g**) and

quantification (**h**) analyses of J3/J2 using anti-J3 antibody in seedlings and buds of Col, *hcr3*, *j3-1*, *j3-3* and *j2-2*. J3/J2, seedling Col ($n = 5$), *hcr3* ($n = 5$), *j3-1* ($n = 5$), *j3-3* ($n = 5$), *j2-2* ($n = 5$); bud Col ($n = 3$), *hcr3* ($n = 3$), *j3-1* ($n = 3$), *j3-3* ($n = 3$), *j2-2* ($n = 3$). Immunoblots of tubulin and Coomassie blue staining were used for loading control and quantification. Black dots represent the normalized intensities of immunoblot replicates. $n =$ the number of independent experiments. Red dots and horizontal lines indicate mean ± s.d. of intensities of immunoblot replicates (two-sided Welch's *t*-test). **i,j**, Representative images (**i**) and quantification (**j**) of flowering time in Col, *hcr3*, *j3-1*, *j3-3* and *j2-2*. Black dots represent leaf numbers of individual plants and red dots and horizontal lines indicate mean ± s.d. values of leaf numbers from individual plants (two-sided Welch's *t*-test).
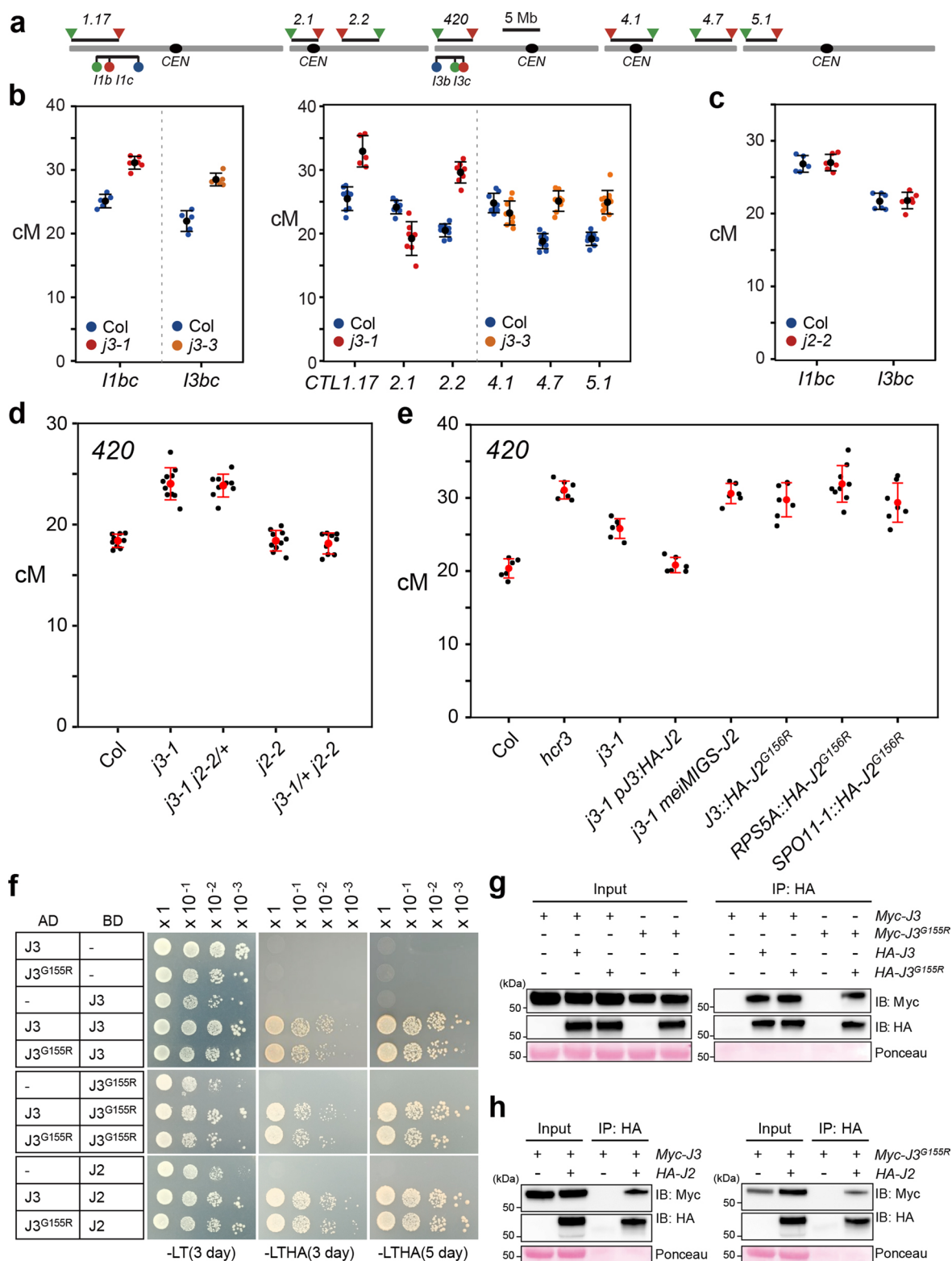
Extended Data Fig. 2 | Functional redundancy between *J3* and *J2* in meiotic crossover frequency. a, Seed (triangles) and pollen (circles) FTLs across the *Arabidopsis* genome. Lines represent the interval positions. **b,c**, Crossover frequency (cM) of pollen (**b**) and seed (**c**) FTLs in Col, *j3-1*, *j3-3* and *j2-2*. **d**, *420* crossover frequency (cM) in Col, *j3-1*, *j3-1 j2-2/+* and *j3-1/+ j2-2*. **e**, As for (**d**) but showing Col, *hcr3, j3-1, j3-1 J3::HA-J2* (T₁), *j3-1 meiMIGS-J2* (T₁) and transgenic plants (T₁) expressing *HA-J2^{G156R}* under the *J3, RPS5A* and *SPO11-1* promoters. Coloured
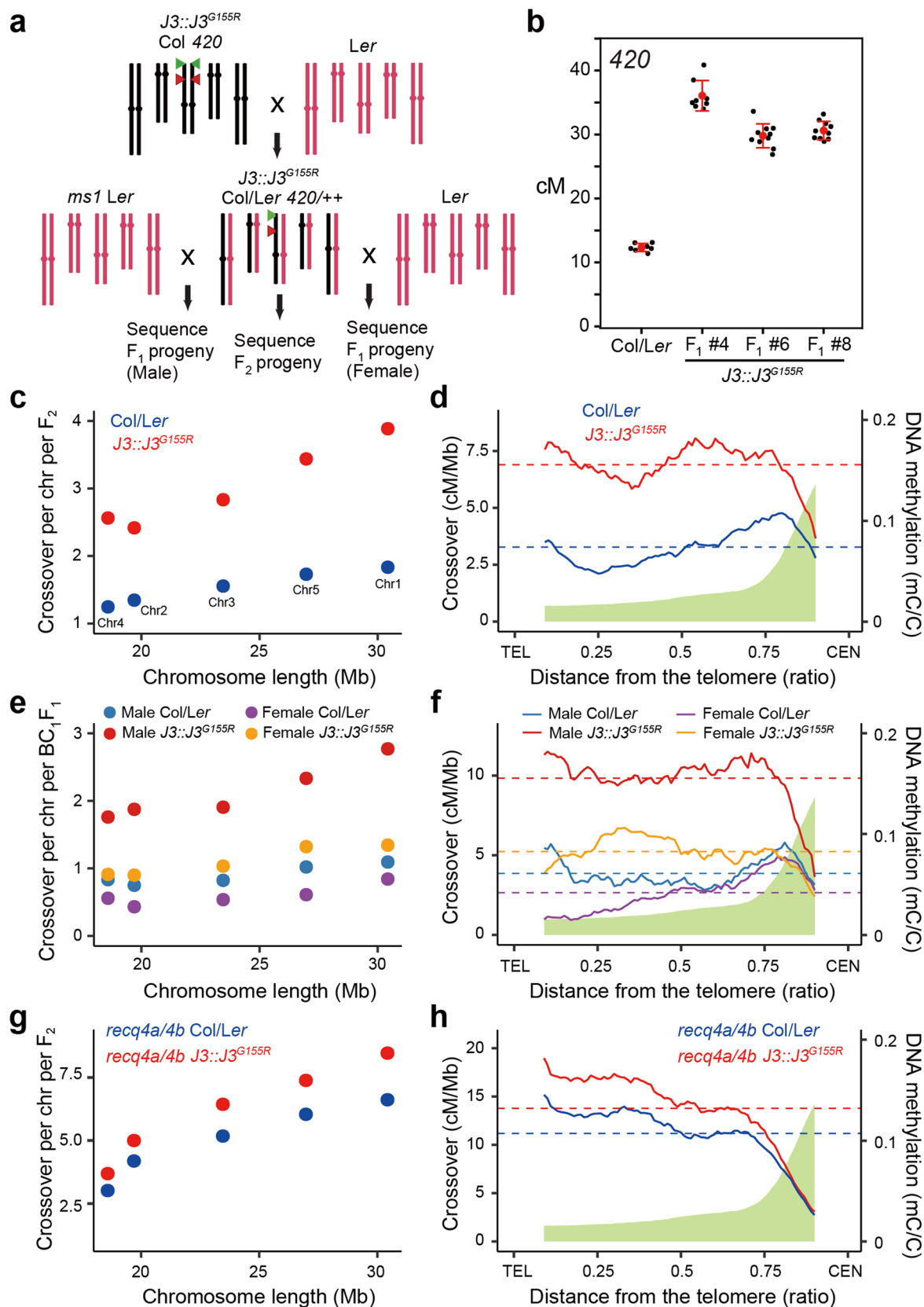
(**b,c**) or black (**d,e**) dots represent cM values of individual plants. *n* = the number of individual plants. Black (**b,c**) or red (**d,e**) dots and horizontal lines indicate mean ± s.d. of cM values from individual plants (two-sided Welch's *t*-test). **f**, Yeast two-hybrid analysis showing protein interactions of J3 and J3^{G155R} with themselves and J2. **g,h**, Co-immunoprecipitation analysis showing dimerization of J3 and J3^{G155R} with themselves (**g**) and J2 (**h**) in *Arabidopsis* protoplasts.

a

Col   hcr3   j3-1   j3-3

j2-2   j3-1 j2-2/+   j3-1/+ j2-2

c

Col   hcr3   j3-1   j3-3   j2-2   j3-1 j2-2/+   j3-1/+ j2-2

b

d

e

genotype	j2-2	j3-1/+ j2-2	j3-1 j2-2	
number	51	57	5	113
ratio (%)	45.1	50.4	4.4	100
genotype	j3-1	j3-1 j2-2/+	j3-1 j2-2	
number	38	35	4	77
ratio (%)	49.4	45.5	5.2	100

j3-1 j2-2/+   j3-1 j2-2

j3-1/+ j2-2   j3-1 j2-2

f

n=58 n=47 n=58 n=56 n=109 n=62 n=24

Col   hcr3   j3-1   j3-3   j2-2   j3-1 j2-2/+   j3-1/+ j2-2

■ Normal   ■ Chromosomal abnormalities

j3-1   j3-1 j2-2/+

j3-3   j3-1/+ j2-2

**Extended Data Fig. 3 | See next page for caption.**

Extended Data Fig. 3 | Functional redundancy between *J3* and *J2* in pollen development, embryogenesis and meiotic chromosome segregation. a,b, Anthers containing Alexander-stained pollen grains (**a**) and plot (**b**) showing viable pollen grains per anther in Col, *hcr3*, *j3-1*, *j3-3*, *j2-2*, *j3-1 j2-2/+* and *j3-1/+ j2-2*. Scale bars, 100 µm. Black dot indicates viable pollens of individual anther. Red dot and horizontal lines indicate mean values ± s.d. values of viable pollens for genotype. *n* = the number of individual anthers. **c,d**, As for (**a,b**) but showing representative images (**c**) and plot (**d**) for number of seeds per silique. White asterisks indicate aborted seeds. Scale bars, 1 mm. Blue and red dots indicate

numbers of plump and aborted seeds per silique, respectively. Black dot and horizontal lines indicate mean values ± s.d. values of seed numbers for genotype. *n* = the number of individual siliques. **e**, Table of genotyping results and representative images showing seedling lethality of *j3-1 j2-2* from the progeny of self-fertilized *j3-1 j2-2/+* and *j3-1/+ j2-2*. Scale bars, 1 mm (top), 1 cm (bottom). **f**, As for (**e**) but showing plot and representative DAPI-stained images of chromosomal abnormalities at metaphase I or anaphase I. Red arrows indicate chromosome fragmentation or interlock. Scale bars, 5 µm. (**b,d**) Data are presented as mean values ± s.d. (two-sided Welch's *t*-test).

Extended Data Fig. 4 | Genomic analyses for crossover number and distribution in Col × Ler and *J3::J3^{G155R}* Col × Ler. a, Schematic of generation of *J3::J3^{G155R}* Col × Ler hybrid plants and crossover map populations. **b**, *420* crossover frequencies in Col × Ler (*n* = 7) and *J3::J3^{G155R}* Col × Ler (#4, *n* = 8, #6, *n* = 10, #8, *n* = 10,) F_1 hybrid plants. Black dots indicate cM values of individual plants. Red dots and horizontal lines represent mean ± s.d. of cM values from

individual plants (two-sided Welch's *t*-test). *n* = the number of individual plants. **c**, Average crossover number per chromosome in Col × Ler and *J3::J3^{G155R}* Col × Ler F_2 individuals. **d**, As for (**c**) but showing normalized crossover frequencies (cM/Mb) along chromosome arms from the telomere (TEL) to the centromere (CEN). **e**,**f**, As for (**c**,**d**), but showing male and female meiosis. **g**,**h**, As for (**c**,**d**), but showing *recq4a recq4b* background.
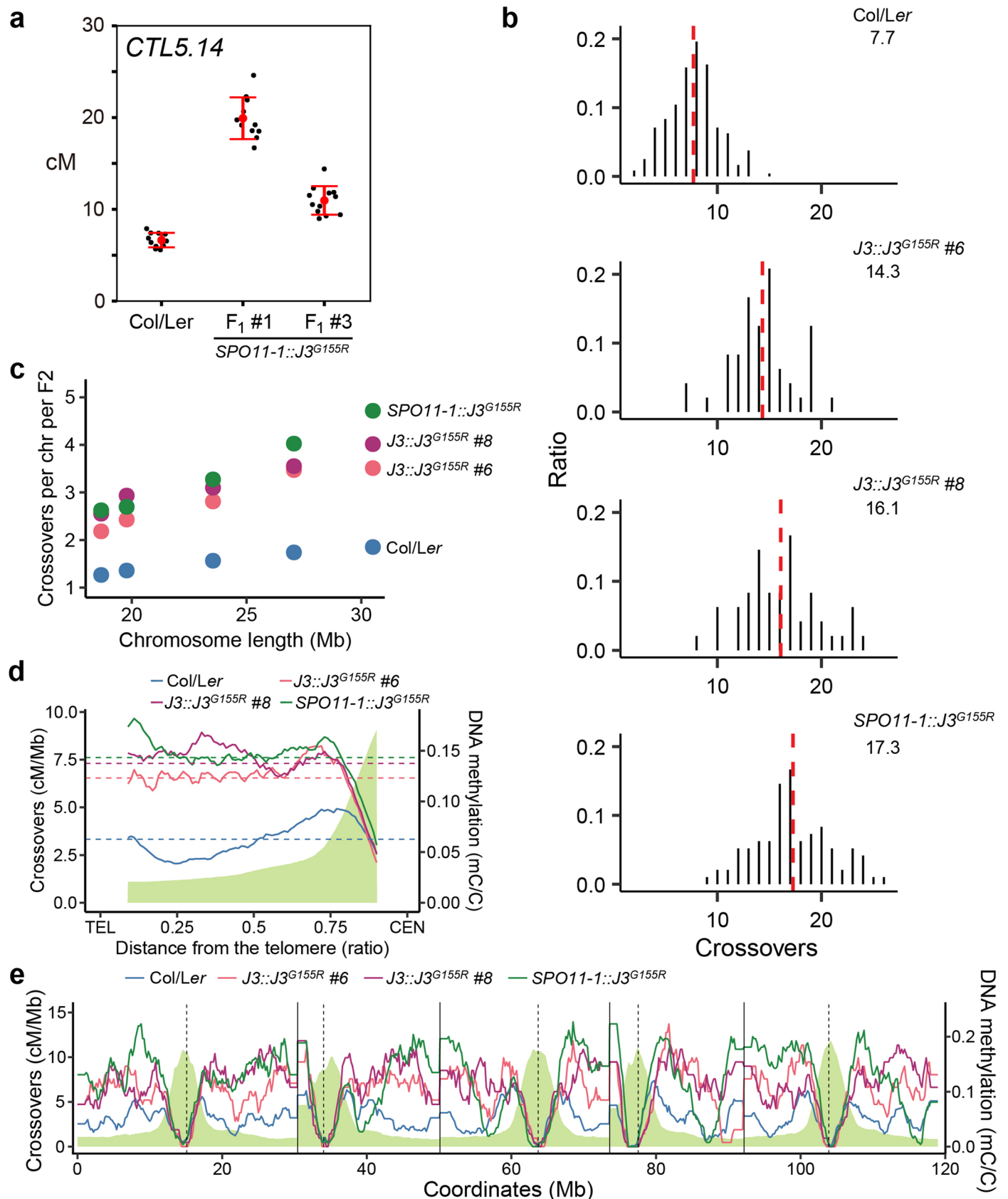
Extended Data Fig. 5 | Genomic crossover maps for F$_2$ individuals from independent *J3::J3^{G155R}* and *SPO11-1::J3^{G155R}* Col × L*er* plants. a, *CTL5.14* crossover frequencies in Col × L*er* (*n* = 11) and two independent *SPO11-1::J3^{G155R}* Col × L*er* (#1, *n* = 11, #3, *n* = 12,) F$_1$ hybrid plants. Black dots indicate cM values of individual plants. Red dots and horizontal lines represent mean ± s.d. of cM values from individual plants (two-sided Welch's *t*-test). *n* = the number of individual plants.

b, Histograms showing the ratio of F$_2$ individuals containing different crossover numbers in each population. Vertical dotted red lines indicate the mean value. **c**, Average number of crossovers per chromosome in F$_2$ individuals in each population. **d,e**, As for (**c**) but showing normalized crossover frequencies (cM/Mb) along chromosome arms from the telomere (TEL) to the centromere (CEN) (**d**) and across the genome (**e**).
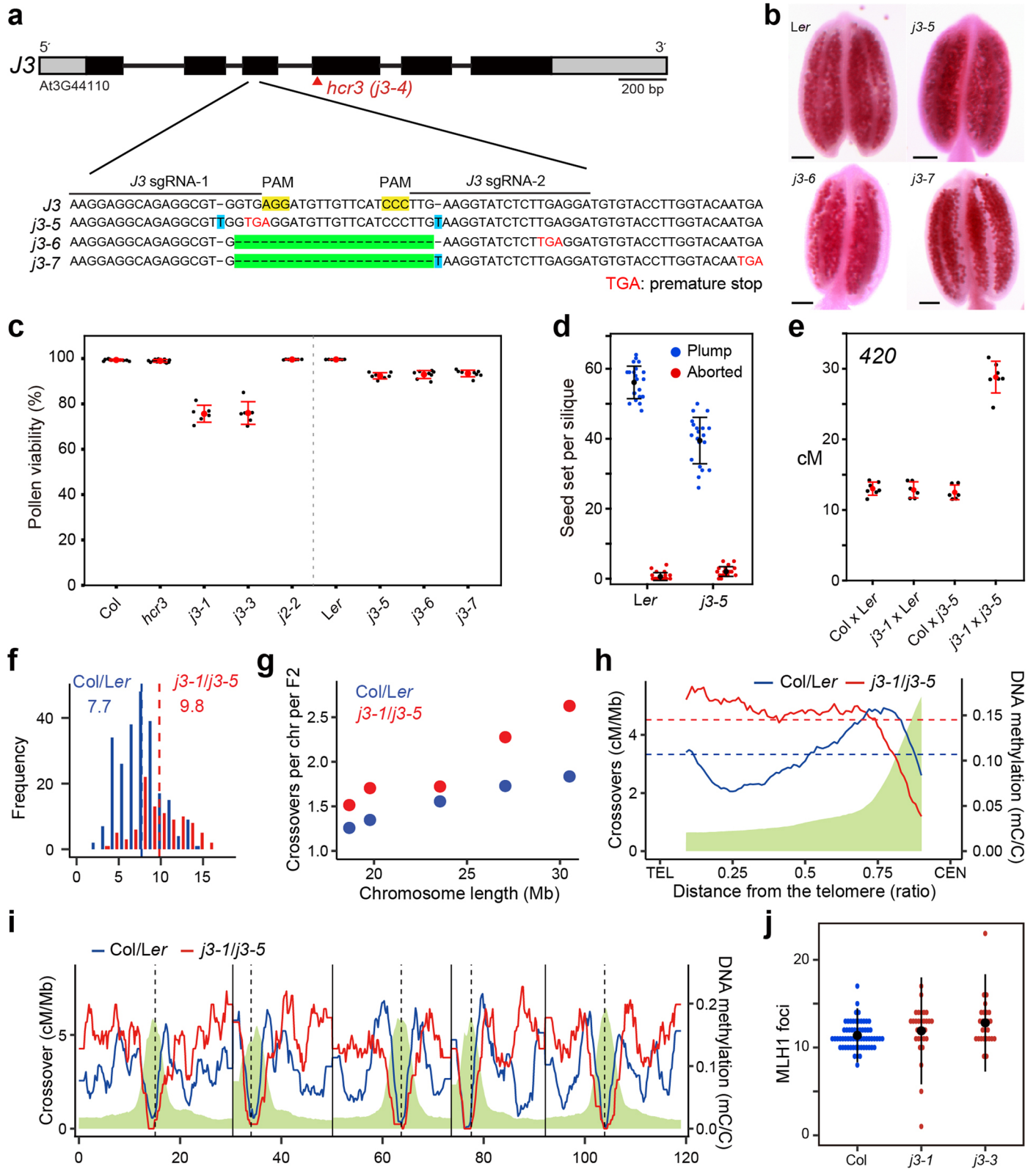
Extended Data Fig. 6 | See next page for caption.

Extended Data Fig. 6 | Genome-wide crossover mapping of *j3* knockout Col × L*er* hybrids and quantification of MLH1 foci in *j3* mutants. a, Gene structure and nucleotide sequences of *J3* with *hcr3* mutation (red triangle), positions of CRISPR/Cas9 sgRNAs and Cas9-mediated mutations for the *j3* null mutants in L*er*. Nucleotide deletions (green), insertions (blue). **b**, Anthers containing Alexander-stained pollens of L*er*, *j3-5*, *j3-6* and *j3-7*. Scale bars, 100 μm. **c**, As for (**b**), but showing pollen viability in Col (*n* = 12), *hcr3* (*n* = 13), *j3-1* (*n* = 6), *j3-3* (*n* = 6), *j2-2* (*n* = 6), L*er* (*n* = 6), *j3-5* (*n* = 7), *j3-6* (*n* = 8) and *j3-7* (*n* = 9). Black dots indicate pollen viability per sample. *n* = the number of independent samples. **d**, Seed number per silique in L*er* (*n* = 23) and *j3-5* (*n* = 21). Coloured dots indicate the numbers of plump (blue) and aborted (red) seeds. *n* = the number of individual siliques. **e**, *420* crossover frequency in Col × L*er* (*n* = 7), *j3-1* × L*er* (*n* = 6), Col ×

j3-5 (*n* = 6) and *j3-1* × *j3-5* (*n* = 7) F$_1$ hybrids. *n* = the number of individual plants. **f**, Histogram of sex-averaged crossover number in Col/L*er* (*n* = 240) and *j3-1*/*j3-5* (*n* = 96) F$_2$ individuals. **g**, As for (**f**), but showing average crossover number per chromosome. **h,i**, As for (**f**), but showing normalized crossover frequencies (cM/Mb) along chromosome arms from the telomere (TEL) to the centromere (CEN) (**h**) and across the genome (**i**). **j**, Quantification of immunostained MLH1 foci of meiotic cells at diplotene stage in Col (*n* = 63), *j3-1* (*n* = 30) and *j3-3* (*n* = 26). Coloured dots indicate numbers of MLH1 foci per cell. Black dots and horizontal lines indicate mean ± s.d. of values of MLH1 foci (two-sided Wilcoxon test, *j3-1 P* = 1.15 × 10^{-2}, *j3-3 P* = 5.88 × 10^{-3}). *n* = the number of independent cells. (**c,d,e**) Data were presented as mean ± s.d. of values and significance was tested by a two-sided Welch's *t*-test.
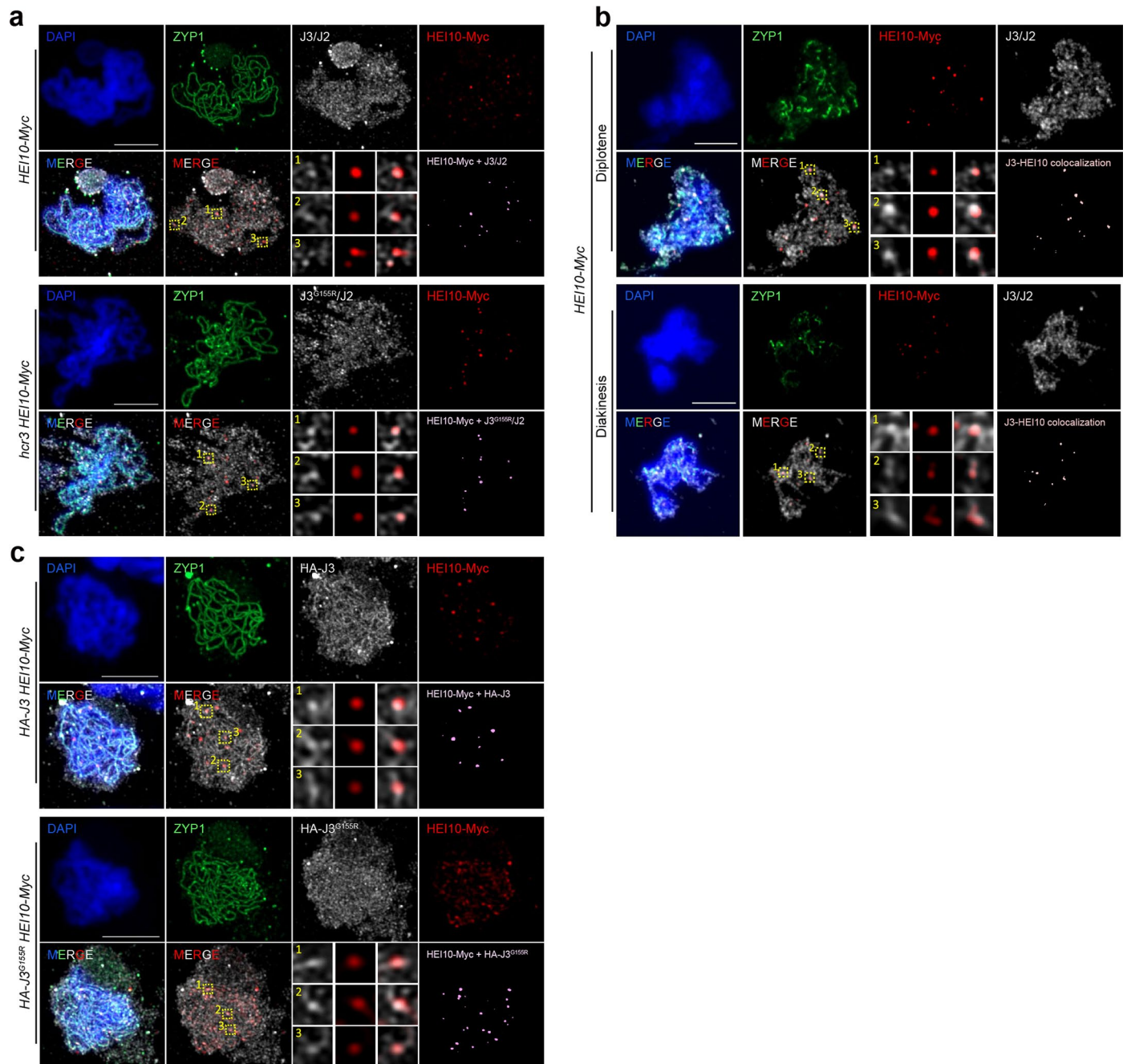
**Extended Data Fig. 7 | J3 and J3^G155R co-localize with HEI10 *in vivo*.**
a, Representative images of co-immunostained J3/J2 (white), ZYP1 (green) and HEI10-Myc (red) at late-pachytene stage in Col *HEI10::HEI10-Myc* and *hcr3 HEI10::HEI10-Myc*. **b**, As for (**a**) but showing at diplotene and diakinesis stage in Col *HEI10::HEI10-Myc*. **c**, As for (**a**) but showing immunostained HA-J3, HA-J3^G155R

and HEI10-Myc at late-pachytene stage in *J3::HA-J3 HEI10::HEI10-Myc* and at mid-pachytene stage in *J3::HA-J3^G155R HEI10::HEI10-Myc* plants. Three yellow dotted line boxes (1, 2, 3) in the merged images of co-immunostained J3/J2 and HEI10 are enlarged and displayed. Scale bars, 5 μm. Experiments (**a**–**c**) were performed at least three times.
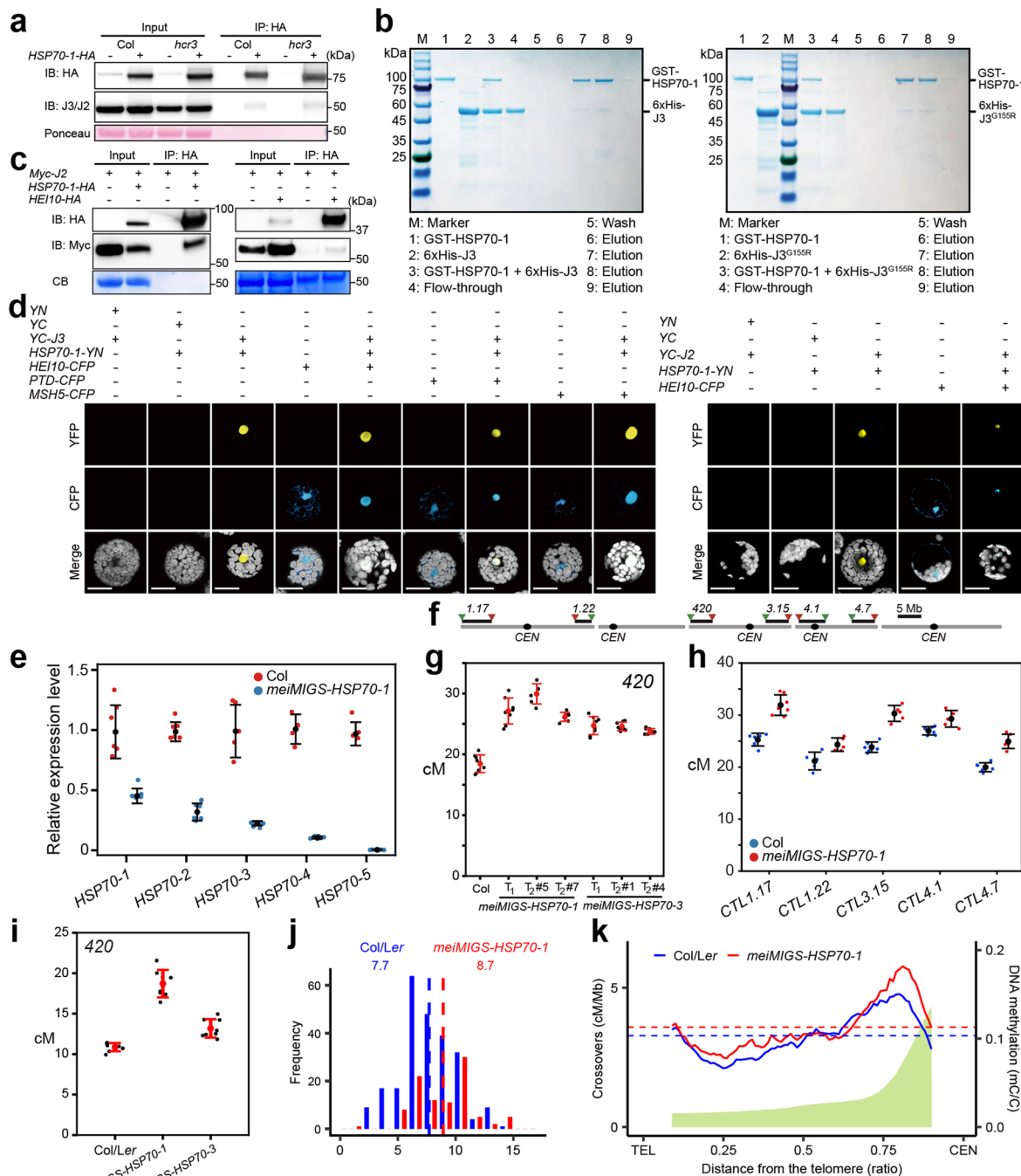
Extended Data Fig. 8 | J3-HSP70 chaperone machinery restricts crossover frequency. a, Co-immunoprecipitation analysis of J3 and HSP70 in *Arabidopsis* protoplasts. **b**, *In vitro* pull-down assay of J3 and HSP70-1. **c**, Co-immunoprecipitation analysis of J2 with HSP70 and HEI10 in *Arabidopsis* protoplasts. **d**, Co-localization of J3/J2 and HSP70 with HEI10, PTD and MSH5 in *Arabidopsis* protoplasts. YN indicates N-terminal 1-158 amino acid resides of yellow fluorescent protein (YFP) and YC, C-terminal 159-238 amino acid residues of YFP for BiFC assay. Scale bars, 20 μm. **e**, RT–qPCR analysis of *HSP70-1-5* genes in unopen flower buds of Col and *meiMIGS-HSP70-1* plants. Red and blue dots indicate two technical duplicates of three biological replicates ($n = 6$ for each genotype) for RT–qPCRs. Mean ± s.d. of values are shown by black dots and horizontal lines. **f**, Seed FTLs across genome. **g**, *420* crossover frequencies in *meiMIGS-HSP70-1* and *meiMIGS-HSP70-3* transgenic lines. *420* Col ($n = 12$), *meiMIGS-HSP70-1* T$_1$ ($n = 8$), *meiMIGS-HSP70-1* T$_2$#5 ($n = 6$), *meiMIGS-HSP70-1*

T$_2$#7 ($n = 4$), *meiMIGS-HSP70-2* T$_1$ ($n = 8$), *meiMIGS-HSP70-2* T$_2$#1 ($n = 8$), *meiMIGS-HSP70-2* T$_2$#4 ($n = 8$). **h**, As for (**g**) but showing CTLs in *meiMIGS-HSP70-1*. *CTL1.17* Col ($n = 6$), *meiMIGS-HSP70-1* ($n = 7$); *CTL1.22* Col ($n = 5$), *meiMIGS-HSP70-1* ($n = 5$); *CTL3.15* Col ($n = 6$), *meiMIGS-HSP70-1* ($n = 5$); *CTL4.1* Col ($n = 6$), *meiMIGS-HSP70-1* ($n = 5$); *CTL4.7* Col ($n = 6$), *meiMIGS-HSP70-1* ($n = 6$). **i**, As for (**g**) but showing *meiMIGS-HSP70/Ler* hybrid plants. Col/L*er* ($n = 8$), *meiMIGS-HSP70-1/Ler* ($n = 8$), *meiMIGS-HSP70-2/Ler* ($n = 8$). **j**, Histogram of crossover number in Col × L*er* (blue, $n = 240$) and *meiMIGS-HSP70-1 × Ler* (red, $n = 96$) F$_2$ individuals. Dotted blue and red lines indicate mean values. **k**, As for (**j**) but showing normalized crossover frequencies (cM/Mb) along chromosome arms from the telomere (TEL) to the centromere (CEN). Black (**g,i**) or coloured (**h**) dots indicate cM values of individual plants. Red (**g,i**) or black (**h**) dots and horizontal lines represent mean ± s.d. of cM values from individual plants (two-sided Welch's *t*-test). (**g,h,i**) $n =$ the number of biologically independent plants.
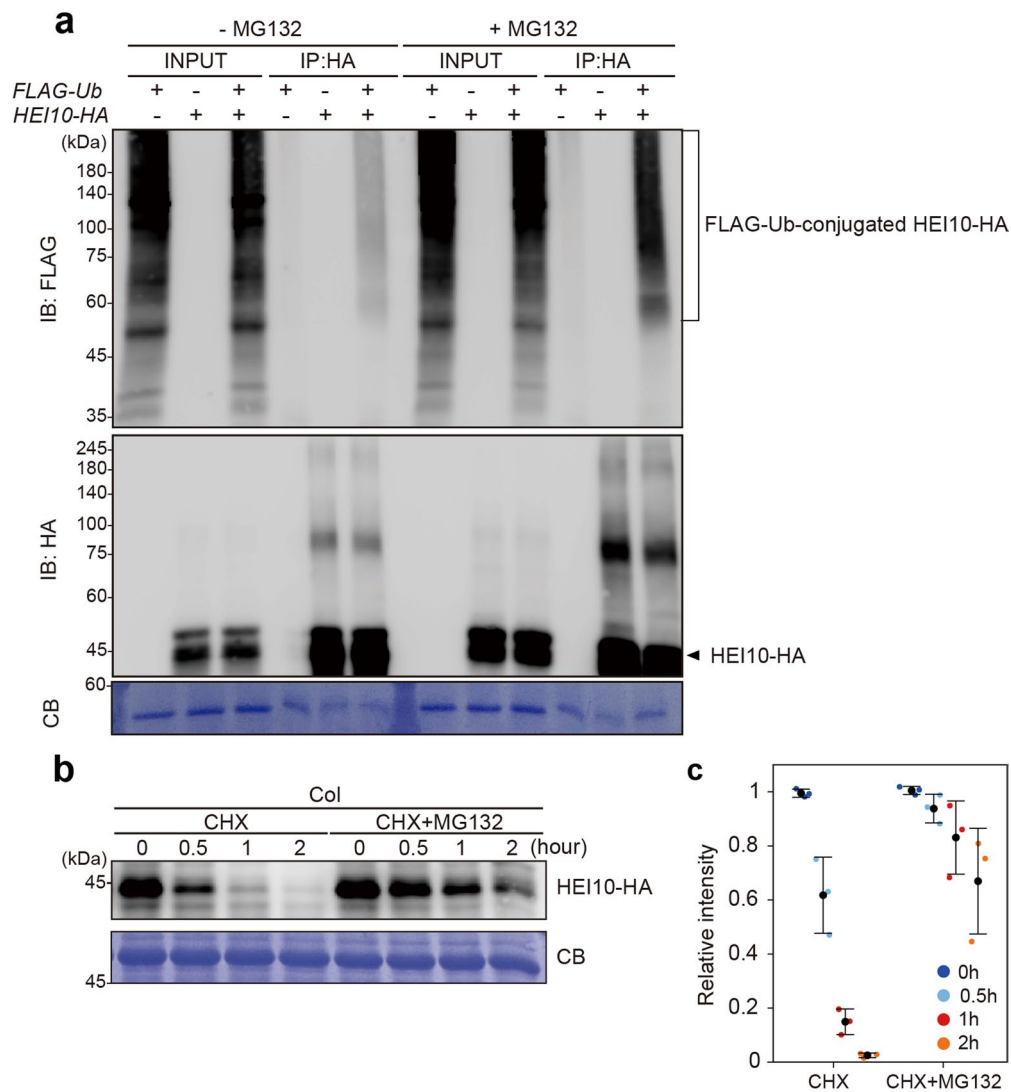
Extended Data Fig. 9 | Ubiquitination modification and proteasome-dependent degradation of HEI10 in *Arabidopsis* protoplasts.
a, Immunoprecipitation and immunoblot analysis of ubiquitin (Ub)-conjugated HEI10-HA in *Arabidopsis* protoplasts. The plasmid constructs for either FLAG-tagged ubiquitin (FLAG-Ub) or HEI10-HA, or both were co-transfected into protoplasts. IP, immunoprecipitation. IB, immunoblot. Coomassie blue (CB) stained membrane is shown as a loading control. Experiments were performed at least three times. **b**,**c**, Immunoblot analysis (**b**) and quantification plot (**c**) of HEI10-HA protein upon treatment of translation elongation (cycloheximide,

CHX) and proteasome (MG132) inhibitors in *Arabidopsis* protoplasts. Coloured dots indicate the normalized intensities of immunoblots. Black dots and horizontal lines indicate mean ± s.d. of values of the normalized immunoblot intensities at 0h (CHX, $n = 3$, CHX+MG132, $n = 3$, $P = 0.47$), 0.5h (CHX, $n = 3$, CHX+MG132, $n = 3$, $P = 4.5 \times 10^{-2}$), 1h (CHX, $n = 3$, CHX+MG132, $n = 3$, $P = 7.3 \times 10^{-3}$) and 2h (CHX, $n = 3$, CHX+MG132, $n = 3$, $P = 2.9 \times 10^{-2}$). Significance between time points was examine using a two-sided Welch's t-test. $n =$ the number of independent experiments.
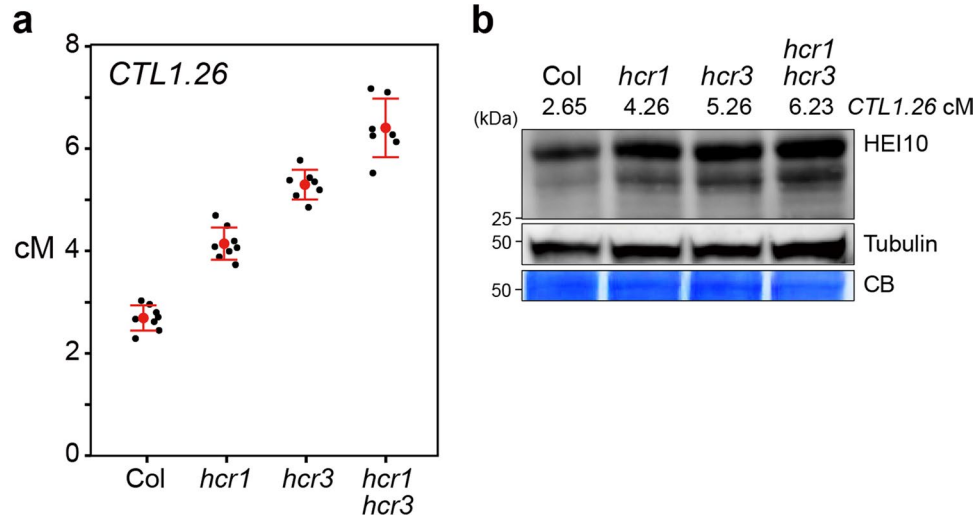
Extended Data Fig. 10 | HCR1 and HCR3 are required for restricting class I crossovers. a, Crossover frequencies of *CTL1.26* in Col ($n = 8$), *hcr1* ($n = 8$), *hcr3* ($n = 7$) and *hcr1 hcr3* ($n = 7$) (Supplementary Table 27). Black dots indicate cM values of individual plants. Red dots and horizontal lines represent mean ± s.d. of cM values from individual plants. Significance between genotypes was tested by a two-sided Welch's *t*-test (Col vs *hcr1*, $P = 1.18 \times 10^{-7}$, Col vs *hcr3*, $P = 4.00 \times 10^{-10}$,

Col vs *hcr1 hcr3*, $P = 2.73 \times 10^{-7}$, *hcr1* vs *hcr1 hcr3*, $P = 6.28 \times 10^{-6}$, *hcr3* vs *hcr1 hcr3*, $P = 1.39 \times 10^{-3}$). $n =$ the number of biologically independent plants. **b**, Immunoblot analysis of HEI10 in Col, *hcr1*, *hcr3* and *hcr1 hcr3*. Coomassie blue-stained membrane and tubulin protein blot were shown as a loading control. Experiments were performed at least three times.